Development of Methodologies for the Analysis and Optimal Site Selection for Photovoltaic Power Plants

Nissrine MAAD
Master in Geospatial Engineering
Department of Geosciences, Environment and Spatial plannings
Faculty of Sciences of the University of Porto
2025

Development of Methodologies for the Analysis and Optimal Site Selection for Photovoltaic Power Plants

Nissrine MAAD

Internship Report carried out as part of the Master in Geospatial Engineering

Department of Geosciences, Environment and Spatial plannings

2025

Supervisor

José Alberto Álvares Pereira Gonçalves, Auxiliary Professor,
Faculty of Sciences of the University of Porto

Co-supervisor

Maria Clara Gomes Quadros Lázaro da Silva, Auxiliary Professor,
Faculty of Sciences of the University of Porto

External Host Supervisor

Rute Isabel Martins dos Santos, Data Engineer, Ceiia

External Host co-supervisor

André Dias, Director of space, Ceiia

Fundação para a Ciência e a Tecnologia

CEiiA

Acknowledgements

I would like to express my sincere gratitude to all those who supported me throughout the development of this dissertation.

First and foremost, I extend my deepest thanks to Professor José Alberto Gonçalves and Clara Lázaro my academic advisors at the University of Porto, for their invaluable guidance.

I would also like to thank Professor Neftali Sillero for his insightful contributions during the Scientific Writing course and for the dedicated meeting to discuss the methodology of this study.

I also wish to thank Rute Santos and André Dias, my supervisors at CEiiA, for their valuable guidance, technical support, and encouragement throughout the internship.

My sincere appreciation goes to the entire CEiiA Space Digital team, especially Cristina, who welcomed me as one of their own and created an inspiring environment of collaboration, trust, and professional growth.

I gratefully acknowledge the Fundação para a Ciência e a Tecnologia (FCT) for the financial support through the research scholarship granted for the development of this dissertation at CEiiA.

I thank the University of Porto and CEiiA for making this work possible and for their contribution to advancing sustainable research and innovation.

A heartfelt thanks to my family, especially my husband and children, for their patience, understanding, and unconditional love. Your support has been my anchor.

Resumo

A crescente procura por energia renovável destaca a necessidade de uma localização eficaz e sustentável de quintas fotovoltaicas Solares (QFs). Este estudo apresenta uma metodologia de apoio à decisão espacial para a seleção ótima de locais para instalação de QFs e para a avaliação da distribuição atual e planeada destas infraestruturas em Portugal continental.

A abordagem é estruturada em duas fases principais. Primeiro, uma fase de restrição aplica uma máscara binária de exclusão que integra dez critérios legais, ambientais e infraestruturais — como áreas protegidas, declive, corpos hídricos e proximidade a aglomerados populacionais — eliminando os terrenos inadequados. Em seguida, uma fase de classificação ordena as áreas remanescentes em quatro classes de adequação, utilizando um modelo de decisão multicritério ponderado com base no Processo Analítico Hierárquico (AHP). O método considera a irradiação solar, o acesso rodoviário e à rede elétrica, bem como a sensibilidade ecológica. A atribuição de pesos foi fundamentada em prioridades legais e lógica espacial, sendo a consistência verificada através do índice de Saaty.

Os resultados indicam que apenas 19% do território continental português é adequado para QFs, dos quais apenas 15% são classificados como adequados ou altamente adequados. As zonas com maior potencial concentram-se no interior sul, em especial no distrito de Évora, que apresenta mais de 2000 km² de área adequada. À escala municipal, apenas 12 municípios atingem a classe mais elevada de adequação.

A sobreposição com localizações reais de QFs revela que mais de 50% das instalações ocorrem em zonas restritas num cenário estrito, e mais de 30% permanecem nessas zonas mesmo sob um cenário mais permissivo. Esta discrepância evidencia um desfasamento crítico entre o potencial técnico e as estratégias atuais de implementação, sublinhando a necessidade de um planeamento mais informado espacialmente e de uma maior coerência entre a política energética e a realidade territorial.

Palavras-chave: Avaliação de sustentabilidade, Quinta solar fotovoltaica, Análise SIG, Tomada de decisão multicritério (MCDM), Processo Analítico por Hierárquia (AHP), Mapeamento de adequação solar

Abstract

The growing demand for renewable energy highlights the need for effective and sustainable siting of photovoltaic farms (PVFs). This study presents a geospatial decision-support methodology for optimal solar farm site selection and the evaluation of current and planned PVF deployment in mainland Portugal.

The approach consists of two main phases. First, a restriction phase applies a binary exclusion mask that integrates ten legal, environmental, and infrastructural constraints—such as protected areas, slope, water bodies, and proximity to settlements—filtering out unsuitable land. Second, a classification phase ranks the remaining areas into four suitability classes using a weighted multi-criteria model based on the Analytical Hierarchy Process (AHP). The method considers solar irradiance, road and power grid access, and ecological sensitivity. Weighting was derived from regulatory priorities and spatial logic with consistency being verified using Saaty's ratio.

Results show that only 19% of Portugal's mainland is suitable for PVFs, with just 15% classified as suitable or highly suitable. High-potential areas are concentrated in the southern interior, particularly Évora district, which contains over 2000 km² of suitable land. At the municipal scale, only 12 municipalities reach the top suitability class.

An overlay with real-world PVF locations reveals that more than 50% of installations are situated within restricted zones under a strict scenario, and more than 30% remain within such zones even under a more lenient one. This discrepancy underscores a critical gap between technical potential and current deployment strategies, calling for spatially informed planning and stronger alignment between policy and territorial realities.

Keywords: Sustainability assessment, Photovoltaic Solar Farm, GIS analysis, Multi-Criteria Decision-Making (MCDM), Analytical Hierarchy Process (AHP), Solar suitability mapping.

Table of Contents

List of Figures

List of Abbreviations

λ_{max} The largest eigenvalue. 41

AHP Analytic Hierarchy Process. iv, 4, 6– 10, 30, 31, 33– 40, 42, 43, 45, 46, 54– 56, 58, 62, 63

ALOS Advanced Land Observing Satellite. 13, 17

APA Agência Portuguesa do Ambiente. 3

ASTER Advanced Spaceborne Thermal Emission and Reflection Radiometer. 13, 17

CC Classification Critera. 14, 21, 30, 37

CEiiA Centre of Engineering and Product Development. 5, 60

CI Consistency Index. 40, 42, 43

COS Carta de Uso e Ocupação do Solo. vi, 14, 16, 17, 21, 28

CR Restrictive Critera. 14, 30, 44

CRa Consistency Ratio. 40– 43

DEM Digital Elevation Model. vi, 8, 11– 13, 17– 19, 33

DGEG Directorate-General for Energy and Geology. 3

DGPC Direção-Geral do Património Cultural. 14, 19

DGT Direção Geral do Território. vi, 10, 11, 13, 14, 16, 60

DTM Digital Terrain Model. 7

EIA environmental Impact Assessment. 3, 4

EU European Union. 1

F Factor. 30

FCT Fundação para a Ciência e a Tecnologia. 5

GHG Greenhouse Gas. 1

GHI Global Horizontal Irradiance. 12, 22, 34, 57, 58

GIS Geographic Information System. 6– 9, 12, 62

IAPMEI Agência para a Competitividade e Inovação. 5

ICNF Instituto da Conservação da Natureza e das Florestas. 16

INE Instituto Nacional de Estatística. 14, 20

IPCC Intergovernmental Panel on Climate Change. 1

IPMA Instituto Português do Mar e da Atmosfera. 13, 24

IRENA International Renewable Energy Agency, Abu Dhabi. 2

LSI Land Suitability Index. iv, 39, 40, 45

MCDM Multi-criteria Decision Making. iv, 4, 6, 10, 12, 21, 26, 30, 62

MCU Minimum Cartographic Unit. 16

NetCDF Network Common Data Form. 13, 24

PNG Portable Network Graphics. 14, 25

PRISM Panchromatic Remote-sensing Instrument for Stereo Mapping. 13, 17

PV Photovoltaic. 2, 22– 24

PVF Photovoltaic Farm. iv, vi, 5, 28, 44– 48, 50, 56, 58, 59, 61, 62

PVFs Photovoltaic Farms. iv, vi, 4, 5, 28, 39, 44– 46, 49, 50, 52, 53, 55, 62– 64

PVOUT Specific photovoltaic power output. 13, 22, 23, 57, 58

QGIS Quantum Geographic Information System. 12, 13, 18, 25, 31

REN Redes Energéticas Nacionais. 14, 25

RI Random Index. 42

SF Solar Farm. 3, 6, 9, 10, 25, 30, 33

SFs Solar Farm. vi, 3, 4, 8, 10, 11, 33, 55

SHP Shapefile. 13– 15

SNIG Sistema Nacional de Informação Geográfica. 14, 16, 20

SRTM Shuttle Radar Topography Mission. 13, 17

TOPSIS Technique for Order Preference by Similarity to Ideal Solution. 7, 56, 58

UN United Nations. 1

WDPA World Database on Protected Areas. 13, 15, 16

1. Introduction

In his New Year's message for 2025, United Nations (UN) Secretary-General António Guterres reminded that this decade has been marked by deadly heat. The ten hottest years on record all occurred between 2014 and 2024 [1].

The rise in global average surface temperature since the pre-industrial era (1850–1900) has caused a significant accumulation of heat. This increase has led to regional and seasonal temperature extremes, reduced snow and sea ice cover, intensified heavy rainfall, and altered plant and animal habitats. Land areas are warming faster than oceans, and the Arctic is warming more quickly than most other regions. The recent rate of warming has far exceeded the average since the start of the 20th century [2]. According to the latest Synthesis Report from the Intergovernmental Panel on Climate Change (IPCC), human activities—mainly through greenhouse gas emissions—are the unequivocal cause of global warming. The global average surface temperature increased by 1.1°C above 1850–1900 levels during the period 2011 to 2020.

Europe, as one of the most industrialized regions in the world, has a significant historical contribution to global greenhouse gas emissions, which are among the main drivers of global warming. However, the European Union (EU) has also been a leader in many environmental initiatives to mitigate these effects.

The European Green Deal aims to make Europe the first climate-neutral continent by 2050 [3], as shown in Figure 1.1. Climate neutrality means achieving net-zero Greenhouse Gas (GHG) emissions: reducing emissions and offsetting the remaining ones through natural absorption by ecosystems or permanent geological storage. This requires significant emission reductions while enhancing the soil's capacity to sequester atmospheric carbon. The Russian invasion of Ukraine accelerated energy sovereignty policies. In 2022, the EU adopted the REPowerEU Plan to eliminate dependence on Russian fossil fuels well before 2030 [4]. By then, the EU intends to reduce GHG emissions by 55% compared to 1990 levels. Such a drastic reduction in such a short time frame will require profound and transformative changes in our energy systems.

The expansion of renewable energy production capacity is thus a key strategy for achieving a climate-neutral continent by 2050. Solar, wind, and hydroelectric energy represent the main renewable sources.

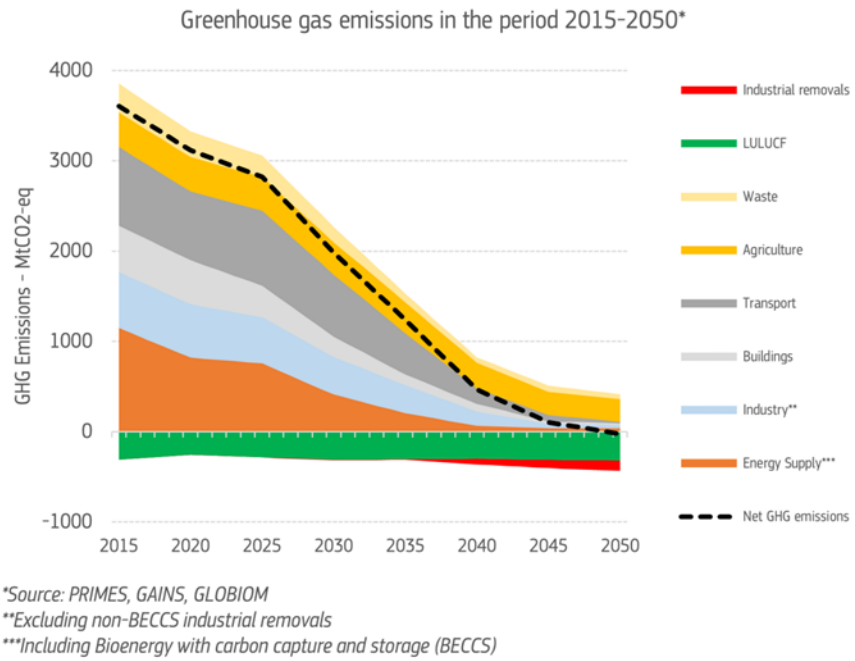

Figure 1.1: Greenhouse gas emissions from 2015 to 2050. (Source: European Commission “2040 climate target”, 2024)

Photovoltaic (PV) solar energy has emerged as one of the most effective and affordable technologies for electricity generation [5], particularly after cost reductions in PV systems, making the technology viable at scale and often independent of subsidies [6, 7].

According to 2024 reports of the International Renewable Energy Agency, Abu Dhabi (IRENA) [8] and the Energy Institute [9], global installed solar capacity grew from 1.2 GW in 2000 to 1.42 TW in 2023. This represents an annual growth rate of 32.2% in recent years and 25.9% over the last decade. China leads this development with 609.9 GW in 2023, 43% of global capacity, and a 55. 2% annual growth rate since 2013.

In Europe, incentive policies and strict carbon emission reduction targets have fueled the rapid expansion of PV solar energy. PV technology has become a key part of the European energy mix. Installed solar capacity rose from 0.2 GW in 2000 to 299.2 GW in 2023, representing a 23.1% annual growth rate. Leading countries include:

- **Germany:** 81.7 GW in 2023 (5.8% of global solar capacity), with a 21.1% annual growth rate.
- **Spain:** 31 GW in 2023, with a 21.1% annual growth rate and around 2.2% global share.
- **Italy:** 29.8 GW, contributing around 2.1% of global capacity.

These advances result from continued investment and public policy that support large-scale plants and access to the electric grid for new solar projects.

In Portugal, solar capacity remains modest compared to global and European leaders, yet it is growing rapidly. The installed capacity for electricity generation increased by 29.3% between 2013 and 2023 and by 46.5% in the last year alone. In January 2024, 81% of Portugal's electricity consumption came from renewable sources: hydropower contributed 47%, wind 25%, biomass 5%, and solar 4%. Net energy imports represented 5% of monthly consumption [10].

These figures reflect Portugal's commitment to reducing fossil fuel dependence and increasing the use of clean energy, directly contributing to its carbon neutrality goals. The recent exponential growth underscores the strategic role of solar energy in the national energy matrix and in the broader context of sustainability and decarbonization.

The current distribution of Solar Farm (SFs) in Portugal, illustrated in Figure 2.1, shows where solar installations are located. They appear scattered throughout the country with no specific pattern in terms of topography or latitude. This suggests that location decisions were likely driven by local feasibility and land availability rather than a unified strategy based on solar potential or proximity to electric grid infrastructure.

However, expanding these installations requires an integrated approach that involves optimal site selection, automatic Solar Farm (SF) detection, and ecological impact assessment. Recent legislative changes, including Council Regulation 2024/223 of 22 December 2023 [11], introduced exemptions from certain environmental evaluation obligations for renewable energy projects essential to electric grid integration [4].

Currently, SF installation authorization in Portugal is regulated by Decree-Law No. 96/2017 of August 10 [12], classifying electrical installations into three types (A, B, C) based on installed capacity and project complexity. Higher capacity installations (types A and B) require an operation certificate from the Directorate-General for Energy and Geology (DGEG).

Moreover, large and complex installations must undergo an environmental Impact Assessment (EIA) issued by the Agência Portuguesa do Ambiente (APA), which evaluates potential ecological, social, and economic impacts. This ensures that SF location and operation comply with environmental and regulatory criteria, minimizing harm to protected areas, ecosystems, and local communities.

Despite the existing regulatory framework, authorizations and EIA are handled case-by-case, often based on land availability and opportunity. While effective in individual implementation, this lacks a comprehensive, integrated territorial strategy to identify optimal solar sites nationwide.

In practice, factors like solar irradiance, infrastructure proximity, and land use are considered in isolated projects. Still, there is no structured national strategy that integrates these with environmental, topographic, and socio-economic criteria. This results in a scattered distribution of SFs with no clear alignment to areas of highest technical and environmental solar potential.

1.1. Study Objectives Framework and Added Value

The main objective of this thesis is to develop a spatial decision support model to evaluate the suitability of locations for photovoltaic farms Photovoltaic Farms (PVFs) in mainland Portugal and to assess the alignment of actual and planned solar installations with these suitability zones.

The methodology applied in this work is presented in this report, structured as follows:

1. **Background**: A review of relevant literature addressing land suitability analysis for solar energy, including Multi-criteria Decision Making (MCDM), the Analytic Hierarchy Process (AHP), and recent national and European legislative frameworks promoting solar deployment. Case studies from Portugal and other countries are examined to contextualize the methodological approach.

2. **Definition and Acquisition of Data**: Compilation of geospatial data representing five thematic factors relevant to solar siting: energy resource, climate, location, topography, and environment. Restriction criteria based on legal and ecological constraints were also collected.

3. **Data Preparation and Structuring**: Harmonization of all datasets to a common resolution and coordinate system. Application of exclusion masks for restricted zones and classification of suitability factors into standardized classes.

4. **Application of AHP and Suitability Mapping**: Pairwise comparison matrices were constructed using the methodology proposed by Saaty [13] for the AHP, enabling a systematic assignment of weights to each factor based on relative importance

[13]. These weights were validated with appropriate metrics and used to compute a suitability index, resulting in national-level maps.

5. **Evaluation of Actual and Planned PVFs**: A spatial overlay analysis was conducted to compare the distribution of real and approved solar farms with the mapped suitability zones. Installations were categorized based on their presence in restricted areas and in each suitability class under strict and moderate restriction scenarios, providing a spatial performance assessment of current solar planning practices.
6. **Presentation and Discussion of Results**: Analysis of how well existing PVFs align with identified suitable areas, including insights into the implications for future planning, legal enforcement, and energy policy in Portugal.

This study is expected to support more informed decision-making in the deployment of solar energy infrastructure. Identifying optimal locations and evaluating current Photovoltaic Farm (PVF) distribution contributes to improving land-use efficiency, regulatory coherence, and environmental sustainability. The geospatial framework developed herein may also be adapted in future work for other renewable energy planning contexts or to incorporate alternative restriction criteria, adjusted buffer limits, or region-specific weighting schemes, making it applicable to broader renewable energy planning scenarios.

In parallel to the main spatial suitability analysis, a complementary deep learning model **Detect-Solar** was developed to automatically detect existing solar farms using GEOSAT-2 imagery. Although not the focus of this dissertation, this contribution demonstrates the potential of integrating artificial intelligence in future large-scale monitoring and validation of solar energy infrastructure.

This research was carried out as part of an academic internship at Centre of Engineering and Product Development (CEiiA), where the use of **GEOSAT-2** satellite imagery was a key component of the proposed work. The technical expertise and satellite resources made available through CEiiA played an important role in shaping the project's development and future applications.

This work was supported by a research scholarship funded by Fundação para a Ciência e a Tecnologia (FCT), under the scope of the project "Agenda NewSpace Portugal" (No. 02-C05-i01.02-2022.C632305114-00466915), financed by national funds through the PRR – Recovery and Resilience Plan, through Agência para a Competitividade e Inovação (IAPMEI).

2. Background

The selection of ideal locations for photovoltaic SF installations is one of the main challenges for the sustainable expansion of solar energy. Previous studies, as shown in Table 2.1, present a representative selection of relevant publications that highlighted the importance of integrating technical, environmental, and socio-economic criteria in site selection, ensuring not only energy efficiency but also minimizing environmental and social impacts. Methodologies based on MCDM, such as the AHP, have proven effective for site selection studies. These techniques allow geospatial data to be combined with specific weighting factors, resulting in detailed and robust analyses.

Table 2.1: Methodologies and main results of solar potential mapping from previous studies

Reference	Methodology	Criteria	Location	Main Results
Al Garni and Awasthi [14]	Geographic Information System (GIS), AHP	Solar irradiance, proximity to infrastructure (roads, power lines, urban areas), land use	Saudi Arabia	Identified 16% of Saudi Arabia as suitable for large-scale SF installations
Aly et al. [15]	GIS, AHP	Solar irradiance, proximity to water, infrastructure (roads, grid, urban areas, mines), topography, protected areas, land use	Tanzania	For SF, 20,801 km² designated as most suitable, 68,848 km² as suitable, and 78,133 km² as moderately suitable
Asakereh et al. [16]	GIS, AHP -Fuzzy*	Solar irradiance, slope, proximity to water and infrastructure (roads, grid, urban areas), land use	Khuzestan, Iran	8.87% of the area identified as excellent suitability, 9.87% as moderate to suitable
Vrînceanu et al. [17]	GIS, AHP	Solar irradiance, temperature, sunshine duration, wind, slope, topography, proximity to infrastructure (roads, grid), land use, protected areas	Romania	29.9% (71,100 km²) of the country classified as very high or high suitability, 14.8% (35,300 km²) as moderate, 5% (11,800 km²) as low to very low

Continued on the next page

* AHP-Fuzzy: Enhances AHP by incorporating uncertainty in human judgment using fuzzy logic.

Reference	Methodology	Criteria	Location	Main Results
López-Bravo et al. [4]	GIS, AHP	Slope, orientation, minimum required area, land use (protected zones, agriculture, forests, water), infrastructure (roads, grid, urban areas)	Southwest Spain	76% of the study area excluded for cultural and environmental reasons; 21% of the total SF project area is protected
Sindhu et al. [18]	GIS, AHP Technique for Order Preference by Similarity to Ideal Solution (TOPSIS)*	Social (economy and tourism), Technical (solar irradiance, labor, climate), Economic (grid and transport access), Environmental (visual, sound, biodiversity impacts, toxic emissions), Political (public policies, land use)	Haryana, India	Five municipalities ranked from most to least suitable
Spyridonidou et al. [19]	GIS, AHP TOPSIS, Entropy†	Solar irradiance, PV energy output, land use (tourist zones, coast, agriculture, forests, urban areas), minimum area required	Portugal	12 municipalities classified as excellent, 262 as high, and only 3 as low suitability
Mensour et al. [20]	GIS, AHP	Solar irradiance, land use (agriculture), slope, proximity to infrastructure (roads, grid, urban areas, airports, rivers, flood zones)	Southern Morocco	5.38% (2,892.57 km²) very suitable, 0.91% (491.48 km²) low suitability, 15.61% (8,395.74 km²) moderately suitable, and 2.18% (1,174.21 km²) suitable
Finn and McKenzie [21]	GIS, AHP	Solar irradiance (from Digital Terrain Model (DTM)), slope, orientation, proximity to roads, water, protected areas, land use (from Sentinel-2 imagery)	Northern Ireland	10% of the region (392 km²) identified as very suitable

Continued on the next page

* AHP-TOPSIS: Combine the strengths of AHP for weighting and TOPSIS for ranking.

† AHP-TOPSIS-Entropy: Combine subjective AHP and objective (Entropy) weight calculation before using TOPSIS for final ranking.

Reference	Methodology	Criteria	Location	Main Results
Giamalaki and Tsoutsos [22])	GIS, AHP	Solar irradiance, proximity to infrastructure (roads, grid), water, coast, environmental and visual impacts, land use, topography, slope, orientation	Rethymno, Crete	2.88% of the area identified as very suitable
Janke [23]	GIS	Solar irradiance, federal lands, land use, population density, distance to infrastructure (roads, grid, cities)	Colorado, USA	191 km² of the state identified as very suitable
Kowalczyk and Czyża [24]	GIS, AHP	Existing SFs, solar irradiance, PV potential, precipitation, temperature, wind, proximity to infrastructure (roads, grid, urban zones), water, protected areas, minimum area, perimeter and shape, slope	Northeast Poland	176 locations identified with optimal suitability
Tercan et al. [25]	GIS, AHP	Solar irradiance, land use (Corine classification), water bodies, protected areas, distance to infrastructure (roads, grid, cities), slope, orientation, topography	Anatolia, Turkey	3.70% of the region identified as very suitable and 40.01% as moderately suitable
Kranjčić et al. [26]	GIS	Solar panel technology (various types), Digital Elevation Model (DEM), solar irradiance (from DEM), slope, orientation, land use (Corine classification)	Varaždinska, Croatia	20.23 km² of the region identified as very suitable
Potić et al. [27]	GIS, AHP	Solar irradiance (from DEM), cloud cover, temperature, proximity to roads and urban areas, slope, land use (from Landsat-8)	Knjaževac, Serbia	One 0.25 km² site chosen as suitable

Continued on the next page

Reference	Methodology	Criteria	Location	Main Results
Doljak and Stanojević [28]	GIS, AHP	Solar irradiance, sunshine duration, temperature, relative humidity, slope, orientation, vegetation (NDVI)	Siberia	Eight municipalities identified with excellent suitability totaling 82 hectares
Elboshy et al. [29]	GIS, AHP	Solar irradiance, temperature, cloud cover, land use, distance to infrastructure (roads, grid, cities), slope, topography, soil texture	Egypt	Most suitable SF locations are in the southeastern region along the Nile River

Based on the reviewed literature, it is evident that GIS-based Multi-Criteria Decision-Making (MCDM) approaches, particularly the Analytical Hierarchy Process (AHP), are widely adopted for photovoltaic site selection due to their ability to integrate diverse spatial criteria and expert judgment. While methods like TOPSIS and Entropy have been successfully applied (e.g., Spyridonidou et al. 19; Sindhu et al. 18), they present limitations when used independently. TOPSIS, for example, excels at ranking alternatives but relies heavily on pre-defined weights, making it less transparent and potentially less adaptable in early-stage planning. Entropy, on the other hand, provides objective weight calculation by measuring variability among criteria, but it does not incorporate expert or regulatory preferences, which are crucial in national-scale energy planning. Fuzzy AHP, as applied by [16], offers a way to handle uncertainty in expert judgment but adds complexity that may not be justified when input uncertainty is limited or well-defined by regulation.

It is also important to note that only a few studies, namely [14], [15], [20], and [22], explicitly applied a restriction phase to exclude environmentally or legally protected areas before suitability classification using MCDM. Most other works incorporated all criteria simultaneously, potentially leading to methodological inconsistencies in areas subject to strong regulatory constraints.

Given the policy-driven context of this study and the availability of normative and spatially explicit data in Portugal, the AHP method was selected as the most appropriate approach. Its interpretability, ease of integration with GIS, and alignment with decision-making frameworks in spatial planning make it especially suitable. The method enables pairwise comparisons that reflect regulatory priorities, such as land protection, technical feasibility, and environmental sensitivity. In this study, the AHP weighting process

is applied to five main suitability factors, energy resource, topography, location, climate, and environment, following the methodological logic of national studies like [15], but with greater spatial resolution and a more detailed exclusion and classification logic.

By combining this structured AHP-GIS approach with spatial overlay analysis, the present study aims not only to identify optimal areas for new solar farm installations but also to evaluate the coherence of current and planned projects with these suitability criteria. This methodological choice ensures both traceability and practical relevance for sustainable energy planning in Portugal.

Figure 2.1 illustrates the location of existing solar farms up to May 2025, revealing a significant difference between current SF locations and those registered by the Direção Geral do Território (DGT). Current locations were initially identified through visual detection on Google Earth and, in cases where prepared areas were suspected, confirmed using the latest Copernicus satellite imagery. Conversely, the DGT's SF data, obtained from their public platform, may include both existing installations and planned but not yet constructed projects. This discrepancy is primarily due to the inclusion of future developments in the DGT's dataset. In rare cases, photovoltaic installations identified by visual inspection were not found in DGT records.

The presence of both current and planned SFs appears scattered throughout the territory, with no clear pattern based on topography or latitude. This distribution underscores the need for a robust methodology to identify optimal locations for new installations that balance energy efficiency, environmental impact, and economic feasibility.

However, despite the growth of solar energy in Portugal, there remains a lack of systematic approaches that integrate topographic, ecological, and economic data into a unified decision-making model.

This study has two primary objectives. The first is to develop a model to identify ideal sites for the installation of solar farms in mainland Portugal using AHP techniques within the broader context of MCDM. The proposed approach classifies areas based on their suitability, identifying those best suited for infrastructure implementation based on technical, economic, and environmental criteria.

The second objective is to analyze the distribution of existing or planned solar farms in Portugal and evaluate their alignment with the suitability criteria defined in this study. This aims to understand the extent to which current installations align with optimal conditions

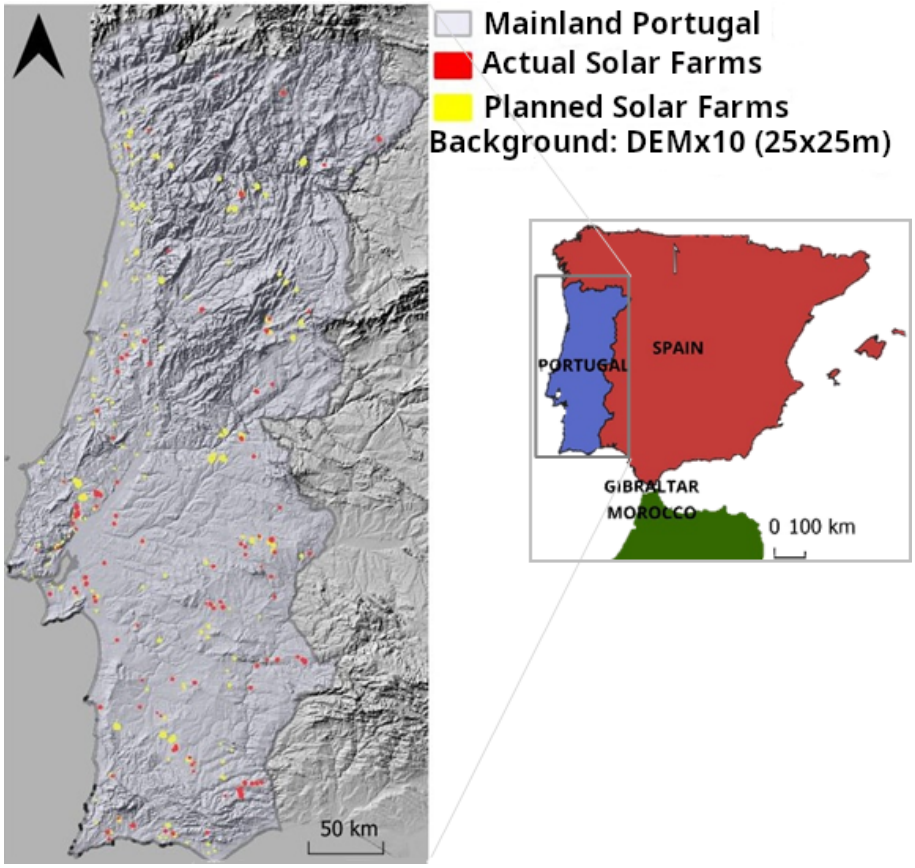

Figure 2.1: Location of the study area and spatial distribution of actual and planned SFs in mainland Portugal. *Note: SF locations as of May 2025. Sources: Actual SFs—author; Planned SFs— DGT. Background: DEM with altitude exaggeration of 10, resolution of 25 m.*

identified through analysis, thereby offering recommendations for future planning.

Based on Portugal's geographic and climatic conditions, the central hypothesis of this study is that the highest solar potential index will be found in the Alentejo region. This is due to the combination of high solar radiation, low population density, predominantly flat terrain, and few dense forested areas (such as eucalyptus) or humid vegetation zones with high carbon stock.

The results of this study are expected to provide solid support for decision-making in the planning of new solar farms in Portugal. The proposed methodology aims to identify sites with high technical and economic potential while simultaneously reducing environmental and social impacts. The implementation of this integrated approach will contribute to the sustainable development of solar energy and the broader global challenges of energy transition.

3. Study Area and Data

3.1. Study Area

The study was conducted in mainland Portugal, a country recognized for its high potential in solar energy generation due to favorable climatic conditions. The country receives approximately 2500–3200 hours of sunlight annually, which translates to an average of 325 sunny days per year [30].

The orography of mainland Portugal ranges from plains in the south to mountainous regions in the north and center, as illustrated by the DEM in the background of the Figure 2.1. This geographic diversity is crucial for modeling and selecting sites for solar installations, considering factors such as slope, solar radiation, land cover, and proximity to electrical infrastructure.

3.2. Data

The data used in this study were collected to create a GIS database in Quantum Geographic Information System (QGIS), containing data layers from various sources, formats, and resolutions, as detailed in Table 3.1. This database supports geospatial analysis aimed at identifying high-potential locations for solar installations while minimizing environmental and social impacts.

In general, the selection of a site for hosting a solar farm must consider environmental, economic, and social aspects. Ideally, the site should be well-irradiated, accessible, and flat. Furthermore, it should not be located in public interest or protected areas. Combining these parameters is highly complex, prompting researchers to rely on a combination of MCDM methods and GIS to tackle this challenge.

Table 3.1: Geospatial data collected for the GIS database

Data	Type	Source	Format	Remarks
Global Horizontal Irradiance (GHI) (KWH/m²)	Meteorological	Global Solar Atlas, 2024 Solargis [31]	Raster (tif)	Long-term annual average, covering 1994–2018. 250 m resolution.

Continued on next page

Data	Type	Source	Format	Remarks
Specific photovoltaic power output (PVOUT) (KWH/KWP)	Meteorological	Global Solar Atlas, 2024 Solargis [31]	Raster (tif)	Long-term annual total average, covering 1994–2018. 1 km resolution.
Air Temperature (°C)	Climatological	Global Solar Atlas [31], Copernicus [32]	Raster (tif)	Long-term annual average, 1994–2018. 1 km resolution.
Relative Humidity (%)	Climatological	Instituto Português do Mar e da Atmosfera (IPMA) [33], Copernicus [32]	Network Common Data Form (NetCDF)	Long-term annual average, 1950–2024. Interpolated data for mainland Portugal. 100 m resolution.
DEM (m)	Orography	CIMAR *, FCUP † [34]	Raster (tif)	Derived from satellite missions: Shuttle Radar Topography Mission (SRTM), Advanced Spaceborne Thermal Emission and Reflection Radiometer (ASTER), Advanced Land Observing Satellite (ALOS)-Panchromatic Remote-sensing Instrument for Stereo Mapping (PRISM), and TerraSAR-X‡.
Slope	Orography	Author	Raster (tif)	Derived from DEM in QGIS. 25 m resolution.
Aspect	Orography	Author	Raster (tif)	Derived from DEM in QGIS. 25 m resolution.
Special Protection Zones	Environmental	World Database on Protected Areas (WDPA) [35], DGT [36]	Vector Shapefile (SHP)	National, regional, and international protection zones.

Continued on next page

*CIMAR: Interdisciplinary Centre of Marine and Environmental Research
†Faculdade de Ciências da Universidade de Porto
‡TerraSAR-X: Terra Synthetic Aperture Radar, X- band

Data	Type	Source	Format	Remarks
Land Use	Environmental, Safety, and Infrastructure	DGT [37], Sistema Nacional de Informação Geográfica (SNIG) [38]	Vector SHP	Carta de Uso e Ocupação do Solo (COS)2018 updated in 2023.
River Network	Environmental	DGT[39]	Vector SHP	Data from 20/11/2024.
National Heritage	Cultural-Historical	Direção-Geral do Património Cultural (DGPC) [40].		
Population Census	Socioeconomic	Instituto Nacional de Estatística (INE) [41]	Vector SHP	Clusters of more than 10 dwellings. 2021 data revised in 2024.
High Voltage Grid	Infrastructure	Redes Energéticas Nacionais (REN)-HUB [42]	Image (Portable Network Graphics (PNG))	Digitized from georeferenced image. Data from 31/12/2022.
Road Network	Infrastructure	OpenStreetMap [43]	Vector SHP	Data from 20/11/2024.
Current and Planned Solar Farms	Energy Resources	DGT [44]	Vector SHP	Data from 12/12/2016.
Current Solar Farms	Energy Resources	Author	Vector SHP	Digitized from Google Earth imagery and complemented with recent Sentinel-2 images. Data from 30/11/2024.

In this study, ten Restrictive Critera (CR) and five classification factors, subdivided into nine Classification Critera (CC), were defined. In a decision-making process, each criterion represents a measurable aspect of an evaluation that enables the characterization and quantification of the alternatives.

These criteria were carefully selected based on a literature review, legal consultations

regarding photovoltaic installation licensing procedures, and reports from environmental impact assessments of solar park projects. Regional specifications of mainland Portugal were also considered in the selection of criteria, ensuring that the analysis is both relevant and adapted to the specific context.

3.2.1 Restrictive Criteria

Before detailing the specific criteria, it is essential to understand what constitutes a Restrictive criterion in the context of this study. Restrictive criteria are parameters that disqualify locations from being considered viable for the development of solar farms. They are applied to ensure that the selected areas do not compromise significant environmental, cultural, or social values.

The following section details each Restrictive criterion used in the study, describing not only their relevance to the assessment but also the specific data sources, applied processing methods, and reclassification strategies used to establish precise limits for each restriction. This meticulous approach ensures that the selected sites are not only suitable but also aligned with the rigorous environmental, social, and economic standards required for the sustainable development of solar farms.

1. **Special Protection Zones (CR1)**

   In the context of this study, the constraint criterion for special protection zones is essential to ensure that solar farm installations respect significant environmental values. These zones are defined based on specific legislations and include protection areas at national, regional, and international levels. Information on these areas was obtained from the WDPA [35] portal and provided in vector format SHP.

   According to the Protected Planet portal, Portugal has a total of 439 protected areas, of which 217 have a national designation, covering a total area of 20,962 km². This represents 22.83% of the total mainland territory area, with designations including 49.43% national, 41.69% regional, and 8.88% international. The designation sources are diverse and include:

   - **Ramsar Wetlands of International Importance:** Designated by the Ramsar Secretariat on behalf of the Contracting Parties, updated in 2023.
   - **UNESCO-MAB Biosphere Reserves:** Jointly managed by UNESCO-MAB and UNEP-WCMC, with data updated in 2020.

- **Common Database on Designated Areas:** Provided by the European Environment Agency (EEA), updated in 2024.
- **Natura 2000:** Supervised by the Directorate-General for the Environment (EU) via EEA, with data updated in 2024.
- **OSPAR Marine Protected Areas Network:** Maintained by the OSPAR Commission, based in London, with data updated in 2021.
- **RAMSAR Wetlands (Portugal):** Geographical information provided by Portugal, updated in 2017.
- **UNESCO World Heritage Sites:** Managed by the IUCN World Heritage Programme, updated in 2024.
- **UNESCO-MAB Biosphere Reserves :** Data managed by UNESCO-MAB, updated in 2020.

When integrating the corresponding protected area layers extracted from the DGT SNIG portal [36], discrepancies were identified, such as the absence of certain designated areas in the WDPA database. These discrepancies can be explained by national-level updates, which are confirmed in the data descriptions available on the SNIG portal [39]. Changes to site boundaries are approved by a resolution of the Council of Ministers upon the proposal of the Instituto da Conservação da Natureza e das Florestas (ICNF).

In this study, we opted to retain all polygons corresponding to national, regional, and international protected areas within the national territory (Figure 3.1). An administrative boundary mask for mainland Portugal was applied to retain only terrestrial zones. All these areas are treated as direct exclusion zones, with no additional buffer distance applied. This ensures that solar farms do not interfere with designated environmental protection areas, by the established criteria and applicable legislation, namely European Decree 493/2012 of September 25 [45] and the Spanish Law 2/1989 of July 18 [46].

2. **Water Bodies (CR2)**

   Hydrological information was based on data from the Land Use and Occupation Map (COS), produced by DGT and made available in vector format on the SNIG portal. For this work, the COS2018v2 [39] version was used, offering improvements over v1, with a Minimum Cartographic Unit (MCU) of 1 ha and a minimum distance between lines of 20 m.

Figure 3.1: Spatial distribution of Special Protection Zones in mainland Portugal.

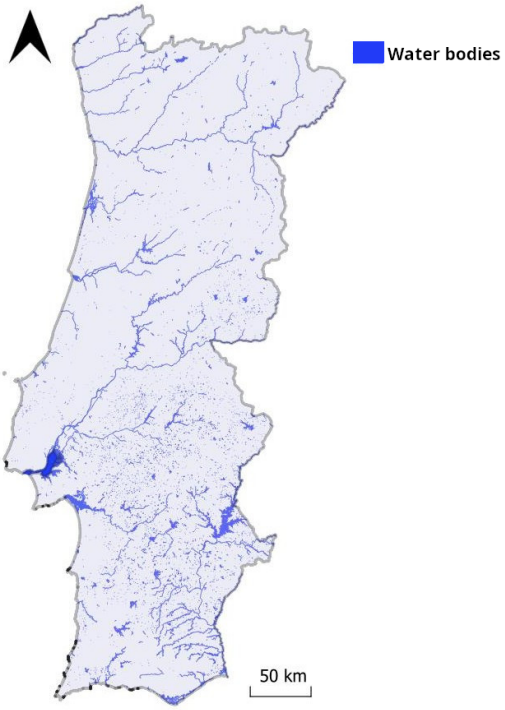

Figure 3.2: Distribution of Water Bodies extracted from COS2018 data.

In this project, all water bodies (Figure 3.2) were considered, including natural or modified watercourses, natural or artificial lakes and ponds, reservoirs, ponds, aquaculture zones, salt flats, coastal lagoons, and river mouths. Due to their significant hydrological relevance, they were deemed appropriate for exclusion even at large scales. All water surfaces were excluded from the analysis, and an additional buffer of 150 m was applied in response to environmental and technical concerns. This distance was selected based on previous studies [15, 17, 19].

3. **Altitude (CR3)**

Altitude information was obtained from a DEM [34] developed using satellite data from SRTM (2000), ASTER (1999), ALOS- PRISM (2006–2011), and TerraSAR-X (2007), available in raster format (.tif) with 25-meter resolution via the website of Professor J.A. Gonçalves. Altitude variability in mainland Portugal is shown in (Figure 3.3).

Locations above 1000 meters in altitude were excluded from potential solar farm sites. This limitation is based on significantly increased investment costs at such altitudes, often rendering projects economically unfeasible. Studies in the literature support the selected threshold [17, 47, 48].

4. **Slope (CR4)**

Slope data were derived from the DEM in QGIS (Figure 3.4) at a 25-meter resolution. For large-scale solar farms, flatter terrain is preferred. Slope critically impacts investment and maintenance costs; steep slopes can increase construction complexity and operational difficulty.

Though no strict consensus exists in the literature on acceptable slope limits for solar farm installation, this study excluded areas with slopes greater than 14% to ensure both technical and economic feasibility. This threshold is based on previous studies [15, 17, 19].

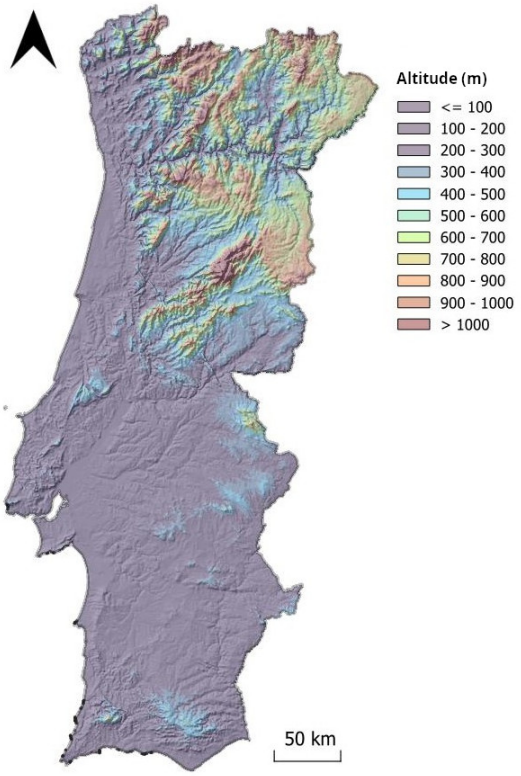

Figure 3.3: Altitude derived from DEM at background x10

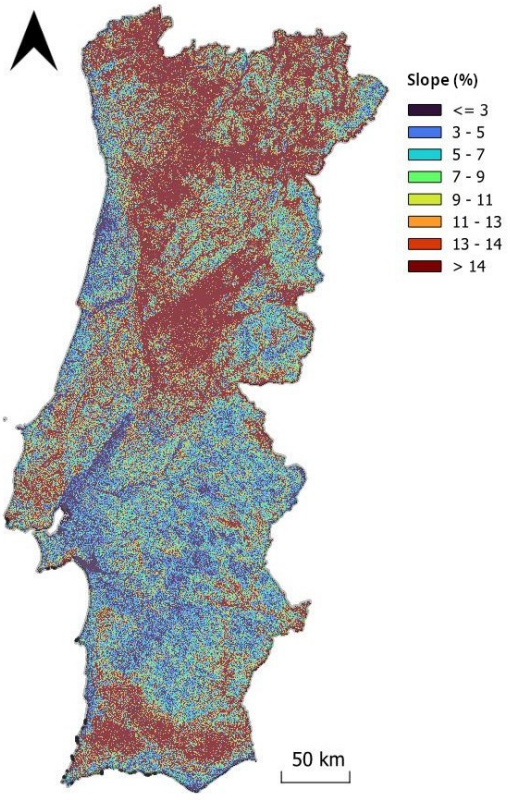

Figure 3.4: Slope derived from DEM.

5. **Aspect (CR5)**

Terrain orientation is crucial when assessing suitability for solar farm installations. Aspect data were derived from the DEM using QGIS at 25-meter resolution (Figure 3.5). South-facing slopes are most suitable for solar energy due to optimal sun exposure.

This study excluded north-facing or near-north-facing slopes, specifically those with aspect between -45° and 315°. However, this restriction was not applied to flat or nearly flat terrains (slope < 3%), where solar panel orientation can be mechanically

adjusted. The constraint becomes critical on steeper terrain, where natural orientation strongly impacts solar capture. This restriction follows findings from [4, 19].

6. **Proximity to Roads and Railways (CR6)**

   Data on road and railway networks were obtained from OpenStreetMap [43], available in SHP format with updates as of November 20, 2024 (Figure 3.6). This study considered all railways and only main, secondary, and tertiary roads, as the primary focus was on the transportation of heavy equipment.

   A minimum distance of 100 m was applied to both networks for safety and visual reasons, while a maximum distance of 10 km was defined to minimize investment costs and environmental impacts. This range is supported by studies [15, 49].

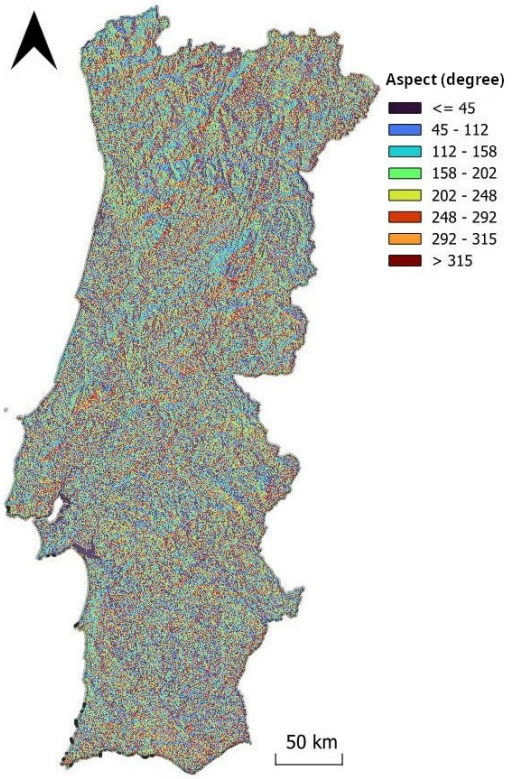

Figure 3.5: Terrain Aspect derived from DEM.

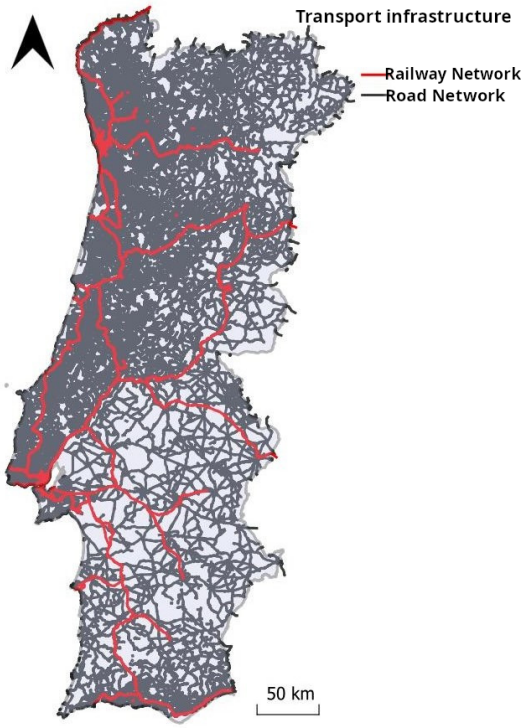

Figure 3.6: Road and Railway Network

7. **National Heritage (CR7)**

   National heritage, including archaeological sites, monuments, and public interest buildings, was extracted from the Cultural Heritage Atlas, managed by the DGPC [40], available in SHP format (Figure 3.7).

   The Portuguese Constitution mandates the protection and valorization of cultural heritage. Law No. 107/2001 of September 8 [50] establishes the framework for this.

In this context, sensitive zones were defined for all archaeological sites, museums, monuments, memorials, castles, ruins, forts, and other relevant cultural assets. A 1000 m buffer was applied around these sites, excluding them from solar installation consideration.

8. **Proximity to Urban and Residential Areas (CR8)**

   Data identifying urban and residential areas with more than 10 housing units were extracted from the Population Census, coordinated by the INE and available on the SNIG portal ("Lugares 2001") [41], with a recent update dated June 20, 2024 (Figure 3.8).

   A safety buffer of 500 meters was applied around these areas to protect the landscape, reduce visual disturbance, and promote social acceptance of solar farm projects.

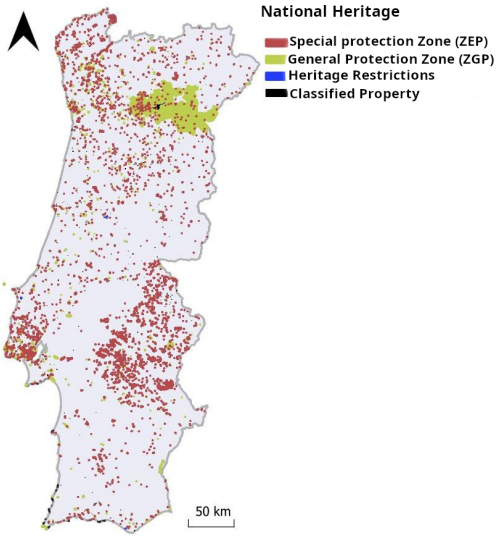

Figure 3.7: Classified and Pending National Heritage Sites.

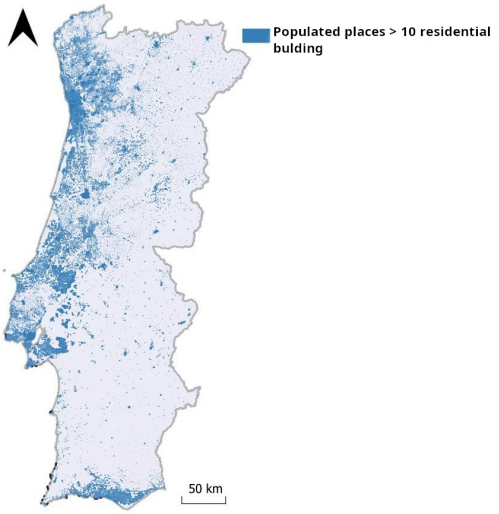

Figure 3.8: Settlement with More Than 10 Housing Units,

9. **Temperature (CR9)**

   Temperature analysis is essential for photovoltaic plant planning since panel efficiency is temperature-sensitive. Using data from the Global Solar Atlas [31] and Copernicus [32], long-term average annual temperature (1994–2018), at 1km resolution, was analyzed (Figure 3.9).

   PV efficiency typically declines linearly with increasing cell temperature: 0.4–0.5% less energy is generated for each 1°C above 25°C [51]. Optimal regions fall within 10–20°C annual averages. Hence, regions below 10°C were excluded.

10. **Proximity to Sensitive Facilities (CR10)**

Sensitive facilities data were extracted from the COS2018 land use data [39]. These include areas such as industry, commerce, agriculture, non-renewable energy production, water supply, waste treatment, ports, shipyards, airports, mines, quarries, landfills, sports and leisure facilities, tourism infrastructure, parks, and cemeteries (Figure 3.10).

All CR10 areas were excluded from PV siting, with a 100 m buffer applied around them.

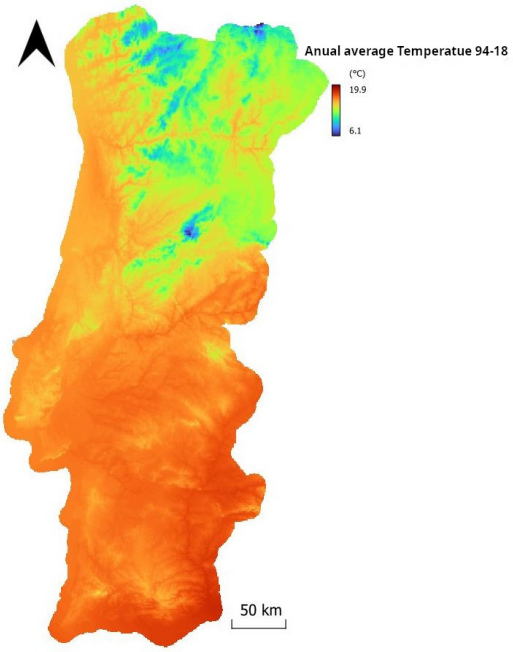

Figure 3.9: Long-term Annual average Temperature.

Figure 3.10: Sensitive facilities

3.2.2 Classification Factors and Criteria

The classification factors and criteria play a crucial role after applying the constraint criteria, being used to evaluate and prioritize eligible sites for the development of solar farms. These criteria are meticulously quantified and implemented through an MCDM. This model calculates values based on the relative importance assigned to each criterion, allowing for a detailed analysis that informs the final site selection.

Each Classification Critera (CC) is analyzed using precise and up-to-date data, which are reclassified and processed to reflect the nuances and specific variations of the study

region. This process ensures that the sites are thoroughly ranked according to the classification criteria assessments, respecting the specific weights assigned to each, thus delivering a precise hierarchy aligned with the strategic objectives of the project.

3.2.2.1 Energy Resource Factor (F1)

This factor focuses on assessing the available energy resources essential for the success of any solar energy installation. It includes criteria such as GHI and PVOUT, which are direct indicators of the energy viability of a site.

1. Global Horizontal Irradiance GHI (CC1)

   GHI in kWh/m² is a fundamental metric for solar energy projects. In this study, it was analyzed using long-term monthly and yearly average values (1994 to 2018) derived from the Global Solar Atlas, Solargis 2024 [31], available in raster format with a resolution of 250 meters. GHI, which measures the solar power received per unit area on a horizontal surface, combines direct irradiance, which hits the surface directly without atmospheric interference, and diffuse irradiance, which is scattered by the atmosphere. This total, known as global irradiance, is crucial for determining the viability of solar farms, especially since sites with high GHI levels are more techno-economically favorable. Large-scale PV installations operate efficiently at annual GHI levels of 1700 kWh/m² or more. The detailed mapping of solar resources in Portugal was reclassified in 100 kWh/m² intervals to guide the selection of ideal energy development sites. Figure 3.11 shows the reclassified GHI map, illustrating irradiation values ranging from 876 to 1921 kWh/m² per year. The relationship between solar irradiance and geographic factors such as latitude, altitude, and terrain orientation was observed, regions with higher altitudes tend to show lower irradiance, while south-facing terrain in Portugal is favored due to maximal solar exposure, reflecting the areas with the highest energy potential for PV investments. Table 4.4 presents the quantitative scoring assigned to the 12 levels of solar irradiance.

2. PVOUT (CC2)

   A key factor considered in this study is the average annual electricity production potential of photovoltaic systems, developed based on Solargis's global solar model. This index, expressed in kWh/kWp, indicates the amount of electricity that would be generated by a PV system with a peak installed capacity of 1 kW. Information

corresponds to long-term, monthly and yearly average values (1994 to 2018) and is available in raster format with a resolution of 1 km, through the Global Solar Atlas [31]. PVOUT is essential for evaluating energy production potential at any location and determining whether a site is suitable for solar project development, as building solar farms in low-potential locations conflicts with their expected performance. The detailed PVOUT mapping for Portugal was reclassified in 100 kWh/m² intervals to support site selection for energy development. Figure 3.12 shows the reclassified PVOUT map, with irradiation values ranging from 900 to 1761 kWh/kWp per year. Notably, the map displays a gradient increasing from north to south, reflecting the influence of latitude and solar irradiance on energy capture efficiency. Southern regions, with greater solar exposure due to their geographic orientation, show the highest PVOUT values. Table 4.4 presents the quantitative scores assigned to the 10 PV potential levels.

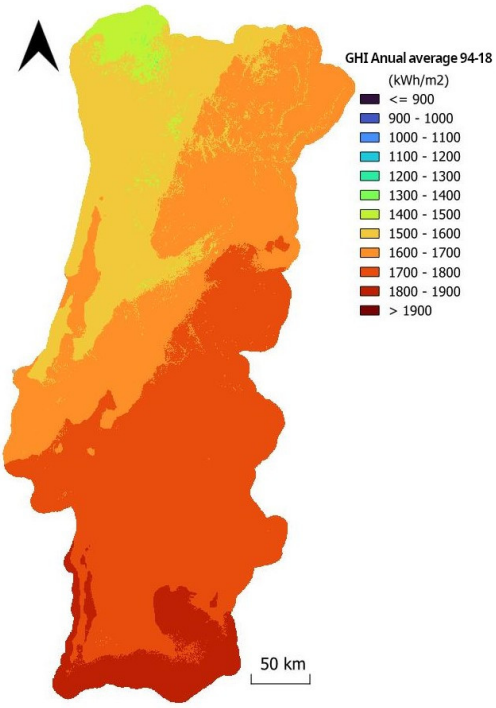

Figure 3.11: Long-term Annual average Global Horizontal Irradiance (GHI).

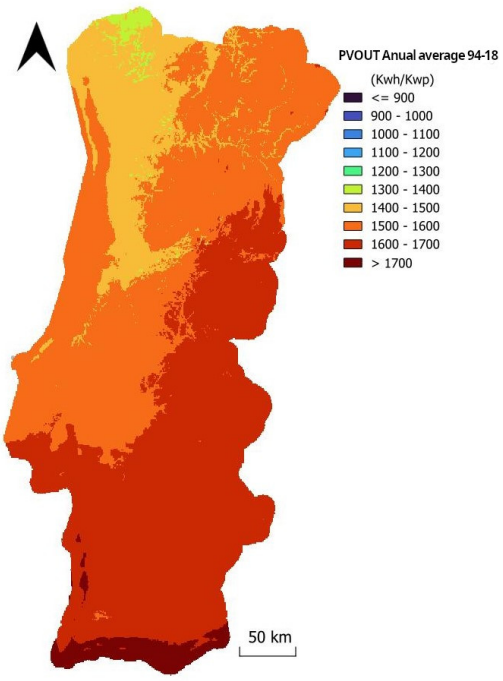

Figure 3.12: Long-term Annual average electricity production potential of photovoltaic systems.

3.2.2.2 Climate Factor (F2)

This factor focuses on analyzing climate conditions that directly affect the operational efficiency and sustainability of solar installations. It includes the criterion of Relative Humidity

(CC3), a crucial indicator impacting both the efficiency of solar panels and the overall viability of the site for solar energy projects.

1. Relative Humidity (CC3)

   Average relative humidity data for mainland Portugal, covering the period 1950 to 2024, were processed using information from IPMA and Copernicus [33], available in NetCDF format with a 100-meter resolution. To analyze the influence of relative humidity on PV performance, a Kriging interpolation was performed in Jupyter Notebook to obtain a more detailed map of this climatic variable.

   Previous studies [52] reported that increased relative humidity is associated with a reduction in the voltage and operating current of solar modules. This is explained by less efficient heat transfer under high humidity conditions, leading to higher operating temperatures and, consequently, reduced energy efficiency. The same authors indicated a 46.2% decrease in energy generation when relative humidity rises from 10% to 50%.

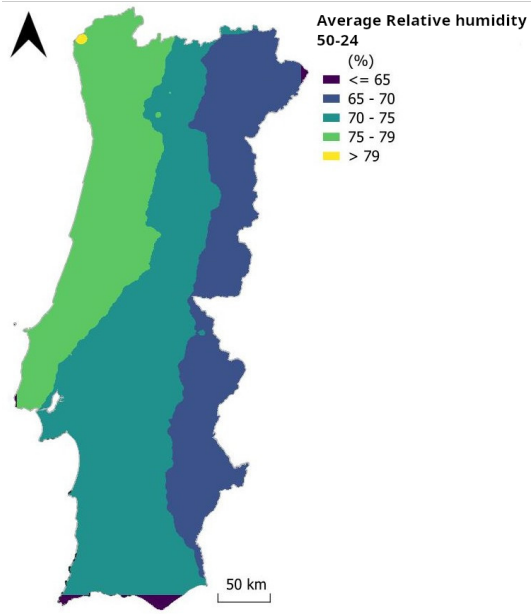

Figure 3.13: Average Annual Relative Humidity

Due to these effects, it is crucial to consider relative humidity when selecting sites for solar development. Areas with lower humidity are preferable to maximize efficiency and energy output. As part of the analysis, the interpolated map of average relative humidity was reclassified to highlight variations in 5% intervals, helping to identify

ideal sites for energy development. Figure 3.13 shows the reclassified map, and Table 4.4 details the quantitative scores assigned to five humidity levels.

3.2.2.3 Location Factor (F3)

This factor analyzes the strategic importance of a location in terms of accessibility and the infrastructure needed for the effective development and operation of SF. It includes key criteria such as proximity to roads, proximity to the electrical grid, and the area required for installing solar farms. Together, these determine the logistical and economic feasibility of potential sites.

1. Proximity to Roads (CC4)

   Proximity to road and rail networks, initially considered a restriction criterion (CR6), is now also used as a classification criterion (CC4) to identify potential sites for solar farm installation. For classification purposes, locations closer to roads are preferred over those further from major road networks. Table 4.4 presents the quantitative scores assigned to five levels of proximity to roads, indicating that the closer a location is to major infrastructure, the more favorable it is considered economically.

2. Proximity to the Electrical Grid (CC5)

   For the development of large-scale solar farms, access to the electrical transmission network is essential, with grid connections typically made at high voltage levels. Data on the high-voltage network were obtained from the REN-HUB portal [42], provided as a PNG image map of high-voltage lines, with information updated to December 31, 2022. The map was georeferenced and digitized in QGIS, as shown in Figure 3.14. For this study, only operational and under-construction high-voltage lines of 150, 220, and 400 KV were considered. Proximity to existing transmission lines is crucial, as being near these infrastructures can avoid additional capital costs and energy losses associated with building new lines.

   Locations near existing or planned transmission networks are preferred due to the economic and logistical benefits they offer. Table 4.4 presents the quantitative scores assigned to five levels of proximity to the electrical grid.

3. Required Area for Solar Farms (CC6)

   In the United States, as mentioned by the Solar Energy Industries Association [53], a typical solar farm requires approximately 2.02 to 4.05 hectares per megawatt (MW)

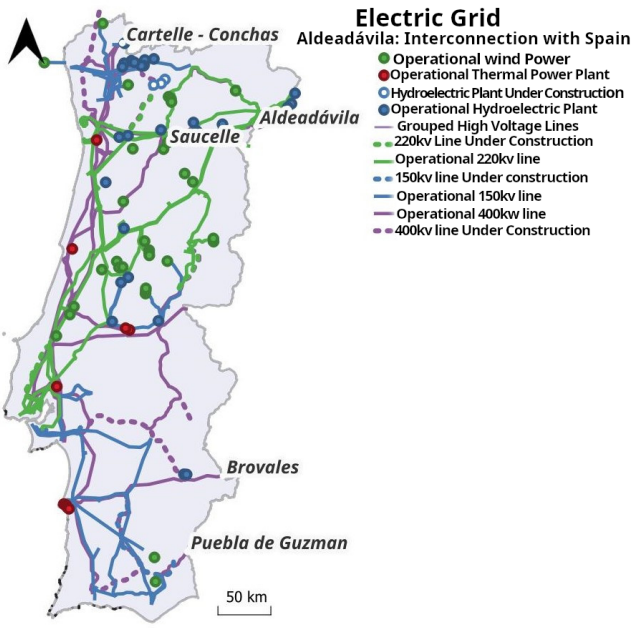

Figure 3.14: Eletrical Grid from [40]

of installed capacity. For commercial or utility-scale projects, the area can reach about 80.94 hectares. This indicates that space requirements can vary widely, but they generally align with the 2.02 to 4.05 hectares per MW range for smaller-scale projects, while large-scale projects may require or exceed 80.94 hectares. In the UK, Lumify Energy [54] suggests a need for about 10.12 hectares for every 5 megawatts of installed capacity. In France, the area needs range from 0.3 hectares for a 0.1 to 0.2 MW installation to 50 hectares for a 20 MW installation, according to the complete guide of solar farms [55].

The most recent study on the subject [4] suggests a minimum required area of 61,430.15 m². In the context of this study, the area required for large-scale solar farms was established as a classification criterion rather than a restriction. An optimal minimum area of 6 hectares was defined to accommodate a large-scale solar farm, based on the operational and logistical needs of such installations. Available areas were thus classified into two main categories: areas above 60,000 m², considered ideal for solar plant development, and areas below this threshold, which may be less suitable for large-scale projects.

This minimum area criterion, specified as 6 hectares, was applied after the MCDM synthesis of the thematic data layers, serving as the final criterion in the evaluation process to ensure that all considered sites have sufficient capacity to accommodate the necessary infrastructure and operate efficiently. This classification is reflected

in Table 4.4, which presents the quantitative scores assigned to these two levels. This classification helps direct development efforts toward areas with real potential to support efficient solar farms, maximizing land use and available natural resources.

3.2.2.4 Orography Factor (F4)

This factor addresses the topographic characteristics of the terrain, which are essential for the efficiency and feasibility of solar farm installations. It includes criteria such as slope and aspect, each of which directly impacts site selection from both construction and energy perspectives.

1. Slope (CC7)

   Slope, initially considered a restriction criterion (CR4), is now also used as a classification criterion (CC7) to assess potential solar farm sites. The slope map, shown in Figure 3.4, was reclassified to illustrate terrain slope variations starting from 2%, facilitating the identification of areas with favorable construction and operational conditions.

   This reclassification is fundamental to understanding how slope influences not only the challenges of earth movement and accessibility but also the potential for energy efficiency and maintenance of solar farms. Table 4.4 presents the quantitative scores assigned to eight slope levels, offering an essential tool for guiding the selection of ideal sites. The various slope levels are assessed to ensure selected areas minimize risks of soil movement and maximize construction and maintenance accessibility.

2. Aspect (CC8)

   Terrain aspect, previously considered only a restriction criterion (CR5), is now also used as a classification criterion (CC8) in the assessment of potential solar farm sites. The reclassification of the aspect map, referenced in Figure 3.5, highlights eight directions from least to most favorable for solar panel installation based on solar capture efficiency.

   This criterion is crucial in determining areas that provide maximum exposure to sunlight, optimizing energy production. Table 4.4 presents the quantitative scores assigned to the eight aspect levels.

3.2.2.5 Environmental Factor (F5)

The Environmental Factor is essential in evaluating the viability of sites for solar farm installation, given that environmental sustainability is a core pillar in implementing renewable energy projects. This factor is especially critical when considering the interaction between land use and environmental conservation, ensuring that solar farm development contributes positively to the landscape and local biodiversity.

In Portugal, the potential deforestation associated with the installation of PVFs has raised increasing concern. Although no systematic analysis was conducted, preliminary visual inspection of Sentinel-2 satellite imagery—comparing scenes before and after PVF installation—suggests that a significant number of these infrastructures were established in forested areas. These observations reinforce the need to consider not only current land use but also the ecological value of existing vegetation in site selection processes.

Therefore, the Environmental Factor focuses on categorizing land according to land use and the ecological relevance of species to minimize environmental impacts. The adopted strategy aims to preserve areas of high ecological value and reduce biodiversity loss, particularly in regions where forests are essential for maintaining ecological balance and carbon sequestration. This is achieved through careful analysis and reclassification of the land use map to identify areas suitable for solar farm installation without compromising sensitive or ecologically important ecosystems.

In this way, solar installations are developed in harmony with environmental conservation goals, contributing to a renewable and ecologically responsible energy future.

1. Land Use (CC9)

   The 2018 Land Use Map (COS2018) [39] was reclassified into six categories for environmental reasons Figure 3.15, aiming to facilitate strategic planning for responsible and sustainable solar farm installation. Artificialized zones considered sensitive and water bodies, treated as restriction criteria (CR11 and CR2, respectively), were excluded to ensure that site selection minimizes environmental impact. The categories are organized as follows:

   - High Environmental Impact Areas – Include cork oak, holm oak, and other broadleaf forests, which are crucial for biodiversity and ecosystem conservation and are significant carbon reservoirs [56], [57], [58].

- Medium-High Environmental Impact Areas – Comprise pine forests, other conifers, and complex cultural mosaics, which maintain a coexistence of agricultural use with natural spaces and contribute to carbon sequestration [59].
- Medium Environmental Impact Areas – Consist of orchards, olive groves, vineyards, and rice paddies, which are culturally and economically important and have limited carbon storage capacity [60], [61], [62], [63], [64], [65] .
- Medium-Low Environmental Impact Areas – Group scrublands, temporary crops, and improved pastures, which provide a transition between high-intensity agricultural zones and areas of higher ecological value, [63], [66].
- Low Environmental Impact Areas – Include agriculture with natural and semi-natural areas and various agroforestry systems that can be adjusted to mitigate environmental impacts, [67], [68].
- Minimal Environmental Impact Areas – Encompass protected agriculture zones, nurseries, and forests with invasive species, offering opportunities for ecological recovery and conversion to solar farms with minimal environmental harm, [69], [70].

Table 4.4 presents the quantitative scores assigned to the six levels of Environmental Impact.

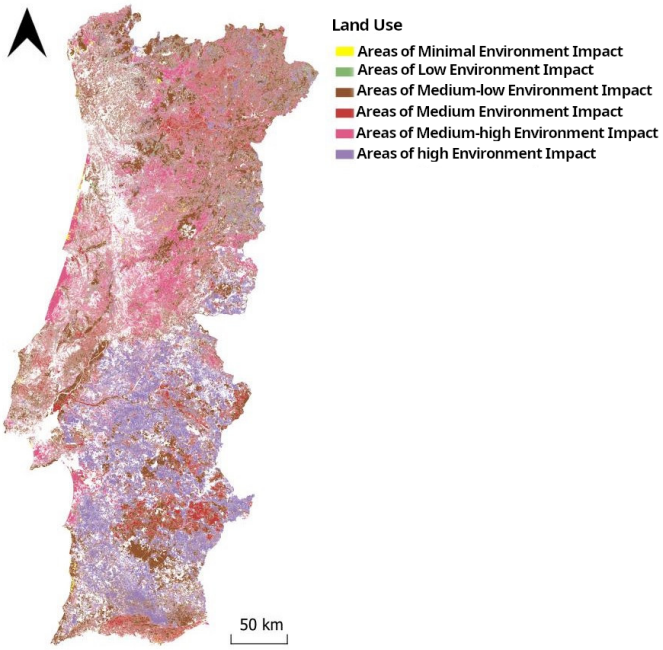

Figure 3.15: Classified land use

4. Methods

In this study, a MCDM approach was employed using the AHP to identify the most suitable locations for large-scale SF installations across mainland Portugal. AHP, developed by Thomas L. Saaty [13], is a structured method grounded in mathematics and psychology that facilitates complex decision-making by breaking down a problem into a hierarchy of goals, criteria, and alternatives. Through pairwise comparisons, it quantifies expert judgment to assign relative weights to each criterion, thus enabling consistent and transparent prioritization.

The analysis followed the steps detailed below.

4.1. Steps of MCDM and AHP Analysis

1. **Determination of Restricted Areas Using Constraint Criteria CR**

   This step involves defining and applying criteria that identify areas where development is prohibited or highly unsuitable, such as environmental protection zones, high-altitude areas, and proximity to sensitive water bodies, defined in the previous section as Constraints Criteria (CR). Areas that do not meet these constraint criteria are excluded from further consideration before any more detailed multi-criteria analysis.

2. **Construction of the AHP Model with Decision Factors and Classification Criteria CC**

   AHP is applied to the areas that passed the restriction phase, where the relative importance of various classification criteria affecting the final decision is evaluated. These criteria may include factors such as proximity to existing infrastructure, energy potential, and environmental impact, defined in the previous section as Decision Factor (F) and Classification Criteria (CC).

3. **Implementation of AHP**

   In this phase, pairwise comparisons of the criteria are conducted to determine the relative weights of each one, which helps to calculate the priority of each site based on all considered criteria.

4. **Application of AHP Results**

The weights derived from the AHP model are applied to the spatial layers representing each criterion to generate a suitability map that indicates the most favorable locations.

5. **Final Decision and Implementation**

   The final decision is based on the suitability map, where the most suitable locations are identified and prioritized for further feasibility studies and potential development.

The methodology applied, as explained in this section, is summarized in Figure 18. All digitization, georeferencing, attribute filtering, layer extraction, and coordinate reference system conversions/harmonizations of the geospatial data were carried out using the open-source software QGIS, version 3.38.3-Grenoble, with GDAL/OGR version 3.9.2. The exclusion of unsuitable areas and the pairwise comparison calculations using AHP were performed with the Python library `pyanp` and the `ahpthree` tool, used within the Jupyter Notebook platform under the Anaconda environment.

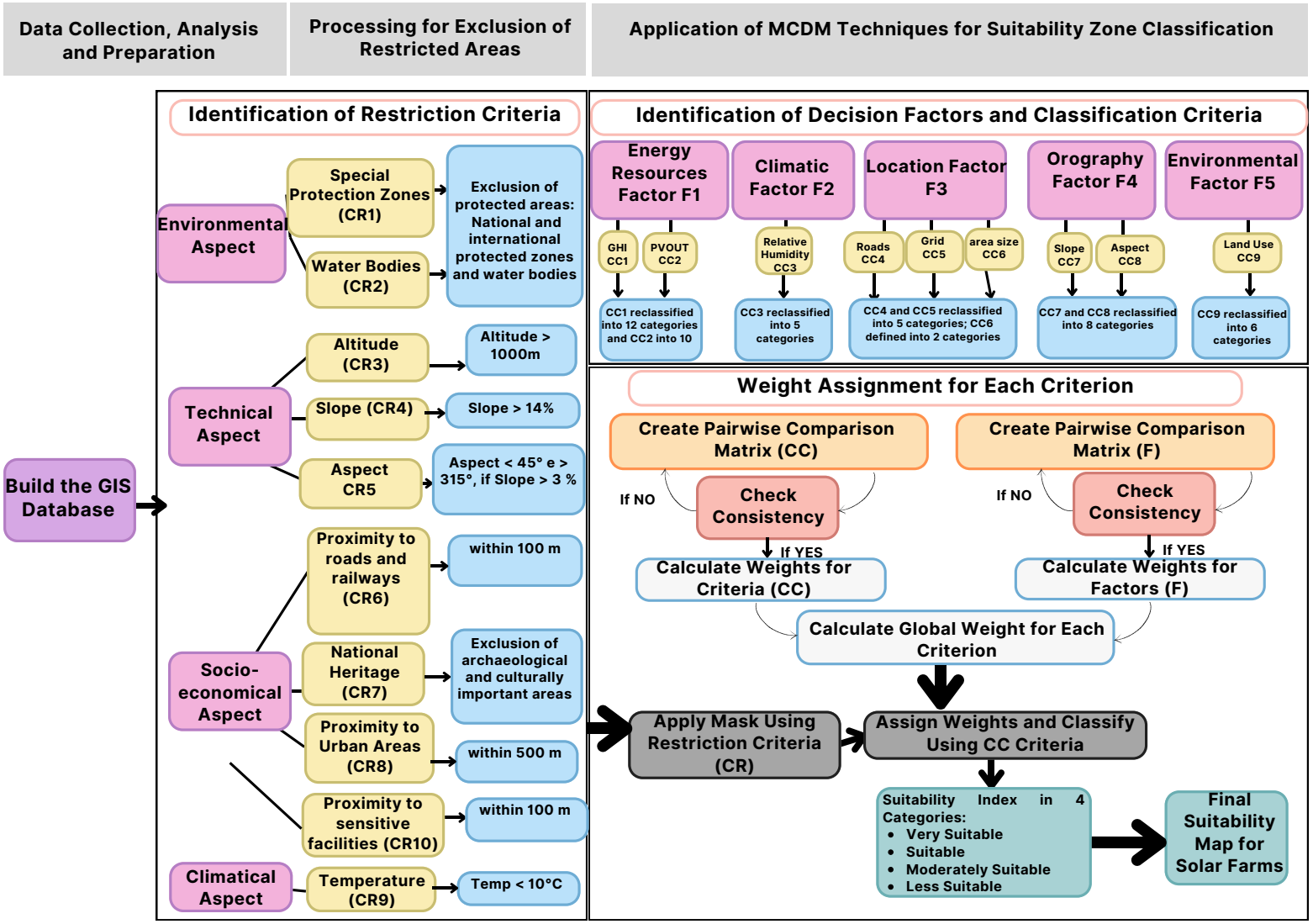

Figure 4.1: Flowchart of the methodology.

4.1.1 Exclusion of Unsuitable Areas

All restriction criteria were used to exclude areas unsuitable for the installation of SFs. First, all layers were rasterized using the DEM as the reference raster, due to its superior resolution in the project. Then, buffers were applied based on the threshold values defined in the flowchart (Figure 4.1). Next, all resulting masks were combined into a single binary restriction mask with values of 0 or 1, corresponding to unsuitable or suitable areas for SF installation, respectively.

In this restriction masking stage, normalization of the criteria was not required, as the goal was simply to exclude areas that did not meet specific predefined conditions. This step is binary, an area either meets a restriction criterion or it does not. For example, an area may be excluded for being within a protected environmental zone or above a certain altitude, without needing to rank these characteristics on a scale.

4.1.2 Construction and Implementation of the AHP Model

The AHP applied in this study followed a systematic approach to prioritize factors, classification criteria (CC), and subcategories of each CC in the context of identifying suitable areas for SF installation. Initially, a structured hierarchy was built to organize the main factors (such as Energy Resources, Climate, Location, Orography, and Environmental), their corresponding classification criteria, and the associated subcategories of each CC.

Pairwise comparisons between elements at each hierarchical level were then conducted, following the methodology developed by Thomas Saaty [13]. This method relies on a numerical preference scale to reflect the relative importance between two elements, ranging from 1 (equal importance) to 9 (extreme importance). Intermediate values (2, 4, 6, and 8) were used for nuanced evaluations between main categories, while reciprocal values (1/2, 1/3, etc.) represented the inverse, such as when one element was deemed less important than another. For example, if a factor was considered five times more important than another (value 5), the reciprocal received 1/5 in the matrix. The upper limit of ”9” aligns with Miller’s Law [71], suggesting that humans can effectively handle 7 ± 2 elements in decision-making processes. Broader scales, like 1–20, not only fail to enhance judgment accuracy but may introduce inconsistencies due to difficulty distinguishing subtle differences among higher values.

1. **Structuring the Pairwise Comparison Matrices at All Levels: Factors, Criteria, and Subcriteria**

   (a) **Factors:** At the top of the AHP hierarchy are the factors, which represent major categories or global objectives that encompass sets of specific criteria. Each factor comprises several criteria that directly contribute to achieving the factor's overall objective. For example, the factor ”Orography” includes the criteria ”Slope” and ”Aspect.”

   The pairwise comparison matrix for the factors is developed by evaluating the relative importance of each factor with respect to the others, thus establishing their priority in the overall project context.

   (b) **Criteria:** Within each factor, criteria represent specific dimensions through which the factor is assessed and operationalized. These criteria are compared within the same factor to determine their relative importance. For example, within the ”Location” factor, the criteria ”Proximity to Roads,” ”Proximity to the Power Grid,” and ”Parcel Size” are evaluated to identify which has the greatest priority or potential impact.

   The pairwise comparison matrices for the criteria reflect how each contributes to the factor under consideration, based on value judgments and priority.

   (c) **Subcriteria:** Subcriteria further detail the criteria, offering a more granular analysis of the specific areas requiring evaluation. They are directly compared using pairwise matrices that assess their relative contribution to achieving the associated criteria.

   Each subcriterion is analyzed to determine its specific weight within the general criterion. For instance, under the criterion ” GHI,” subcategories include: ”<=900,” ”900–1100,” ”1100–1200,” ”1200–1300,” ”1300–1400,” ”1400–1500,” ”1500–1600,” ”1600–1700,” ”1700–1800,” ”1800–1900,” and ”>1900 kwh/m².”

2. **Implementation of Comparison Matrices**

   At each level (factors, criteria, subcriteria), a pairwise comparison matrix is constructed to assess the relative importance of each element concerning the others at the same level. These matrices are fundamental to the AHP decision-making process, as they provide the quantitative basis for calculating the weights that will influence final decisions.

The result of these comparisons is the derivation of priority vectors that are normalized to ensure that the sum of all weights at each level equals one, reflecting the proportional distribution of importance among the evaluated elements.

This hierarchical and systematic approach ensures that all aspects of the decision are considered in an integrated and balanced manner, allowing complex decisions to be made in a structured and justifiable way.

To illustrate the application of the AHP method in this study, representative examples of pairwise comparison matrices are presented for each hierarchical level: factors, classification criteria, and subcriteria. The complete set of matrices is provided in (6).

Table 4.1: Pairwise comparison matrix of the main factors (F).

	F1 (Energy)	F2 (Climate)	F3 (Orography)	F4 (Location)	F5 (Environmental)
F1	1	5	3	7	9
F2	1/5	1	3	5	7
F3	1/3	1/3	1	2	4
F4	1/7	1/5	1/2	1	3
F5	1/9	1/7	1/4	1/3	1

Table 4.2: Pairwise comparison matrix of the classification criteria (CC) within F1 – Energy Resources.

	CC1 (GHI)	CC2 (PVOUT)
CC1	1	3
CC2	1/3	1

Table 4.3: Pairwise comparison matrix of subcriteria for CC1 – Global Horizontal Irradiance (GHI).

	≤900	900–1100	1100–1200	1200–1300	1300–1400	1400–1500	1500–1600	1600–1700	1700–1800	1800–1900	>1900
≤900	1	1	1	1/2	1/3	1/4	1/5	1/6	1/7	1/8	1/9
900–1100	1	1	1	1	1/2	1/3	1/4	1/5	1/6	1/7	1/8
1100–1200	1	1	1	1	1	1/2	1/3	1/4	1/5	1/6	1/7
1200–1300	2	1	1	1	1	1	1/2	1/3	1/4	1/5	1/6
1300–1400	3	2	1	1	1	1	1	1/2	1/3	1/4	1/5
1400–1500	4	3	2	1	1	1	1	1	1/2	1/3	1/4
1500–1600	5	4	3	2	1	1	1	1	1	1/2	1/3
1600–1700	6	5	4	3	2	1	1	1	1	1	1/2
1700–1800	7	6	5	4	3	2	1	1	1	1	1
1800–1900	8	7	6	5	4	3	2	1	1	1	1
>1900	9	8	7	6	5	4	3	2	1	1	1

4.1.3 Calculation of AHP-derived weights

The comparison matrices, referred to in this section as A, are square matrices constructed from pairwise comparisons among factors, criteria, or subcriteria, where each element A_{ij} represents the importance of criterion i relative to criterion j. The main objective of the (AHP) is to extract the relative weights of these criteria in order to support decision-making based on multiple factors.

The process for calculating these weights involves two main steps:

1. **Geometric Mean of Row Entries:**

   For each criterion i, the initial weight w_i is calculated using the geometric product of the entries in the respective row of matrix A. This is done by multiplying all the elements in row i, and then taking the n-th root (where n is the total number of criteria), thus representing the geometric mean:

   $$w_i = \left(\prod_{j=1}^{n} A_{ij} \right)^{1/n} \tag{4.1}$$

   This approach ensures that the initial weight for each criterion reflects the proportional agreement of all its direct comparisons with other criteria.

2. **Normalization of the Weight Vector:**

   After calculating the geometric mean for each row, the resulting weight vector $\mathbf{w}$

is normalized to ensure that the sum of all weights equals 1. This is achieved by dividing each component w_i by the total sum of the vector components:

$$w_i = \frac{w_i}{\sum_{k=1}^{n} w_k} \tag{4.2}$$

This step is essential to convert the relative weights into a standardized and comparable scale, allowing their direct use in the evaluation and prioritization of decision criteria.

This method not only adheres to the structured comparisons in the matrices but also ensures the coherence and precision required for informed decision-making based on multiple interrelated criteria.

Consequently, from the established comparisons, the weights for each factor, CC, and their respective subcategories were meticulously calculated. After determining the weights at all hierarchical levels, the total weight of each subcategory was derived by aggregating the weight of the corresponding factor, the criterion weight, and the subcategory weight.

The results obtained from the AHP processing are detailed in Table 4.4 and Table 4.5. The process was conducted with a firm commitment to transparency, consistency, and clarity in the prioritization of criteria, scientifically supporting the decisions made and ensuring their validity and replicability.

Table 4.4: Normalized priority table, AHP results (Part 1).

Decision Factor (F)	F Weight	Classification Criterion (CC)	CC Weight	Sub-criterion	Sub-criterion Weight	∑ CC (%)
Energy Resources (F1)	0.4353	GHI CC1 (kWh/m²)	0.75	≤900	0.0213	0.0070
				900–1100	0.0184	0.0065
				1100–1200	0.0385	0.0144
				1200–1300	0.0427	0.0156
				1300–1400	0.0520	0.0190
				1400–1500	0.0637	0.0229
				1500–1600	0.0915	0.0298
				1600–1700	0.118	0.0437
				1700–1800	0.1489	0.0485
				1800–1900	0.1789	0.0584
				>1900	0.2191	0.0715
		PVOUT CC2 (kWh/kWp)	0.25	≤900	0.0183	0.003
				900–1100	0.0247	0.003
				1100–1200	0.0635	0.008
				1200–1300	0.0607	0.008
				1300–1400	0.0739	0.008
				1400–1500	0.1075	0.012
				1500–1600	0.1555	0.017
				1600–1700	0.2223	0.024
				>1700	0.3312	0.034
Climate Factor (F2)	0.0584	Relative Humidity CC3 (%)	1.0	≤65	0.436	0.0255
				65–70	0.218	0.0107
				70–75	0.1544	0.0090
				75–79	0.1105	0.0065
				>79	0.081	0.0047

Table 4.5: Normalized priority table, AHP results (Part 2 – continued).

Decision Factor (F)	F Weight	Classification Criterion (CC)	CC Weight	Sub-criterion	Sub-criterion Weight	∑ CC Weights (%)
Location Factor (F3)	0.2002	Distance to roads CC4 (m)	0.2857	≤100	0.0527	0.0031
				100–1000	0.2068	0.0298
				1000–3000	0.1336	0.0136
				3000–5000	0.2050	0.0368
				>5000	0.4020	0.1170
		Distance to power grid CC5 (m)	0.1429	≤1000	0.5128	0.0147
				1000–3000	0.2675	0.0077
				3000–6000	0.1531	0.0045
				6000–10000	0.0333	0.0010
				>10000	0.0333	0.0010
		Area Required CC6 (ha)	0.5714	<6	0.1	0.0114
				≥6	0.9	0.1300
Orography Factor (F4)	0.2002	Slope CC7 (%)	0.5	<3	0.3632	0.0364
				3–5	0.291	0.0315
				5–7	0.1533	0.0193
				7–9	0.0985	0.0099
				9–11	0.0645	0.0071
				11–13	0.0245	0.0026
				13–14	0.0062	0.0007
				>14	0.0006	0.0001
		Orientation CC8 (°)	0.5	158–202	0.3627	0.0363
				112–158	0.1797	0.0179
				202–248	0.1797	0.0179
				248–292	0.1078	0.0108
				292–315	0.0782	0.0078
				45–112	0.0722	0.0072
				>315	0.022	0.0022
				≤45	0.0777	0.0078
Environmental Factor (F5)	0.1059	Land Use CC9 (env. impact)	1.0	Minimal	0.4533	0.0480
				Low	0.2051	0.0217
				Medium-Low	0.1419	0.0150
				Medium	0.0788	0.0084
				Medium-High	0.0383	0.0041
				High	0.0251	0.0027

4.1.4 Land Suitability Index (LSI) Calculation

A territorial suitability index map was developed using a multi-criteria analysis model based on the AHP, implemented entirely in the Jupyter Notebook environment with Python. The objective was to identify potentially viable areas for the installation of PVFs in mainland Portugal.

LSI Calculation Each criterion was represented by a standardized raster, where pixel values were weighted according to the weights assigned through the AHP method. The individual criterion maps were then combined using a weighted sum approach, resulting in the LSI map. The general formula applied was:

$$\text{LSI} = \sum_{i=1}^{n} (\text{Criterion}_i \times \text{Weight}_i) \tag{4.3}$$

This calculation produces a continuous raster in which each pixel contains a value representing its relative suitability.

Normalization of Values To ensure comparability and interpretability, the LSI was normalized to the range $[0, 1]$, where:

- 0 indicates the least suitable areas;
- 1 indicates the most suitable areas.

Suitability Classification For better visualization and interpretation, the normalized index was classified into four suitability levels, each corresponding to an equal range:

- Low suitability (≤ 0.25) – Areas with very limited potential for PVF installation.
- Moderate suitability (0.25–0.50) – Areas with limited viability.
- Suitable (0.50–0.75) – Areas with favorable conditions.
- High suitability (> 0.75) – Areas highly recommended for PVFs.

4.1.5 AHP Model Consistency Validation

To ensure the reliability of the pairwise comparisons in the AHP model, consistency validation tools were applied, namely the **Consistency Index (CI)** and the **Consistency Ratio (CRa)**. These indicators evaluate the logical coherence of the comparison matrices. A matrix is considered consistent when, for example, if criterion A is more important than B, and B is more important than C, then A should also be more important than C.

- **CRa** ≤ 0.10 indicates acceptable consistency.

- **CRa** > 0.10 suggests inconsistency and the need to review pairwise comparisons.

The consistency validation is carried out through a set of structured calculations, detailed as follows:

- **Calculation Steps of** The largest eigenvalue (λ_{max})

  1. **The comparison matrix Normalization** A**:**

     First, the comparison matrix A is normalized to form a matrix of relative priorities. Each element of the normalized matrix $A_{\text{norm}}[i,j]$ is obtained by dividing the original value by the sum of its respective column:

     $$A_{\text{norm}}[i,j] = \frac{A[i,j]}{\sum_{k=1}^{n} A[k,j]} \tag{4.4}$$

     where n is the total number of compared criteria. This step ensures that all columns in the matrix contain proportional and comparable values.

  2. **The weight vector Calculation** w**:**

     The weight vector w represents the relative priority of each criterion in the matrix. It is computed as the average of each row in the normalized matrix:

     $$w[i] = \frac{1}{n} \sum_{j=1}^{n} A_{\text{norm}}[i,j] \tag{4.5}$$

     This vector w is an intermediate step in the derivation of the largest eigenvalue of the matrix, λ_{max}.

  3. **The weighted sum vector Calculation:**

     The weighted sum for each criterion is calculated by multiplying the original comparison matrix A by the weight vector w:

     $$\text{Weighted Sum}[i] = \sum_{j=1}^{n} A[i,j] \cdot w[j] \tag{4.6}$$

  4. **the consistency vector Calculation:**

     The consistency vector is then obtained by dividing each element of the weighted sum vector by the corresponding element of the weight vector:

     $$\text{Consistency Vector}[i] = \frac{\text{Weighted Sum}[i]}{w[i]} \tag{4.7}$$

5. **The largest eigenvalue Calculation λ_{max}:**

   λ_{max} is estimated by taking the average of the elements of the consistency vector:

$$\lambda_{max} = \frac{1}{n} \sum_{i=1}^{n} \text{Consistency Vector}[i] \tag{4.8}$$

- **The CI Calculation:**

$$CI = \frac{\lambda_{max} - n}{n - 1} \tag{4.9}$$

where:

  - λ_{max}: Largest eigenvalue of the comparison matrix.
  - n: Number of elements in the comparison matrix.

- **The CRa Calculation:**

The CRa is obtained by dividing the CI by the Random Index (RI) for the matrix size n:

$$CRa = \frac{CI}{RI} \tag{4.10}$$

Random Index (RI) — tabulated values depending on matrix size n. See Table 4.6 for the RI values as proposed by Saaty [13].

RI Table – Saaty (1977):

Table 4.6: Random Consistency Index (RI) values according to matrix size n, as proposed by Saaty [13].

n	1	2	3	4	5	6	7	8	9	10
RI	0.00	0.00	0.58	0.90	1.12	1.24	1.32	1.41	1.45	1.49

- **Consistency Results**

The consistency validation results for the pairwise comparison matrices are summarized in Table 4.7, which reports the calculated values of λ_{max}, CI, and CRa for each AHP hierarchy level. These values confirm the reliability of the comparison judgments and the weights assigned in the decision-making process.

Table 4.7: Consistency validation results for the comparison matrices.

Matrix	λ_{max}	**CI**	**CRa**	**Interpretation**
F1–F5 (Factors)	5.0204	0.0051	0.0046	✓ Acceptable consistency (CRa < 0.10)
F1 (Energy Resources)	2	0	0	✓ Consistent matrix (only 2 criteria)
F2 (Climate)	1	NaN	0	✓ Only one criterion, consistency check not required
F3 (Location)	3	0	0	✓ Consistent matrix (only 3 criteria)
F4 (Orography)	2	0	0	✓ Consistent matrix (only 2 criteria)
F5 (Environmental Impact)	1	NaN	0	✓ Only one criterion, consistency check not required
CC1 (GHI)	11.288	0.0288	0	✓ Acceptable consistency (CRa < 0.10)
CC2 (PVOUT)	9.408	0.051	0.0352	✓ Acceptable consistency (CRa < 0.10)
CC3 (Relative Humidity)	5.007	0.0017	0.0016	✓ Consistent matrix
CC4 (Roads)	5.0979	0.0245	0.0219	✓ Acceptable consistency (CRa < 0.10)
CC5 (Power Grid)	5.2426	0.0607	0.0542	✓ Acceptable consistency (CRa < 0.10)
CC6 (Required Area)	2	0	0	✓ Consistent matrix (only 2 criteria)
CC7 (Slope)	7.7248	0.1208	0.0915	✓ Acceptable consistency (CRa < 0.10)
CC8 (Orientation)	8.2925	0.0418	0.0296	✓ Acceptable consistency (CRa < 0.10)
CC9 (Land Use)	6.4018	0.0804	0.0648	✓ Acceptable consistency (CRa < 0.10)

Therefore, the analysis of the results demonstrates that all matrices present CRa ≤ 0.10, indicating the absence of significant inconsistencies in the pairwise comparisons. Furthermore, matrices where $\lambda_{max} \approx n$ reflect high coherence in the evaluations performed. For matrices containing only one criterion ($n = 1$) or two criteria ($n = 2$), consistency verification is not required, as there is no room for mathematical inconsistencies.

Thus, the pairwise comparisons are considered consistent, confirming that the derived weights are reliable and can be confidently applied in the AHP model without the need for further adjustments.

5. Results and Discussion

5.1. Mapping the Combined Constraints

The first result obtained in this study was the Combined Constraints Map, which represents the areas of mainland Portugal where the installation of Photovoltaic Farms (PVFs) is unfeasible due to environmental, topographic, and regulatory constraints. This map was generated by overlaying all ten restriction criteria (CR): Special protected zones (CR1), water bodies (CR2), extreme altitude (CR3), slope (CR4) and aspect (CR5), proximity to main roads and railways (CR6), national patrimony (CR7), clusters of population (CR8), extreme temperature (CR9) and sensitive installations (CR10), as shown in Chapter 3 (4).

As illustrated in Figure 5.1, a significant part of the territory presents constraints, particularly in high-altitude regions and protected zones. These areas were excluded from the suitability analysis to ensure that only locations free of critical impediments were considered for optimal PVF site selection.

The restriction mask was applied to the multi-criteria analysis model, ensuring that only pixels classified as unrestricted (value 0 in the data matrix) were included in the suitability assessment. As a result, approximately 73.7% (68,114.25 km²) of the Portuguese territory was classified as unsuitable due to the presence of at least one restrictive criterion.

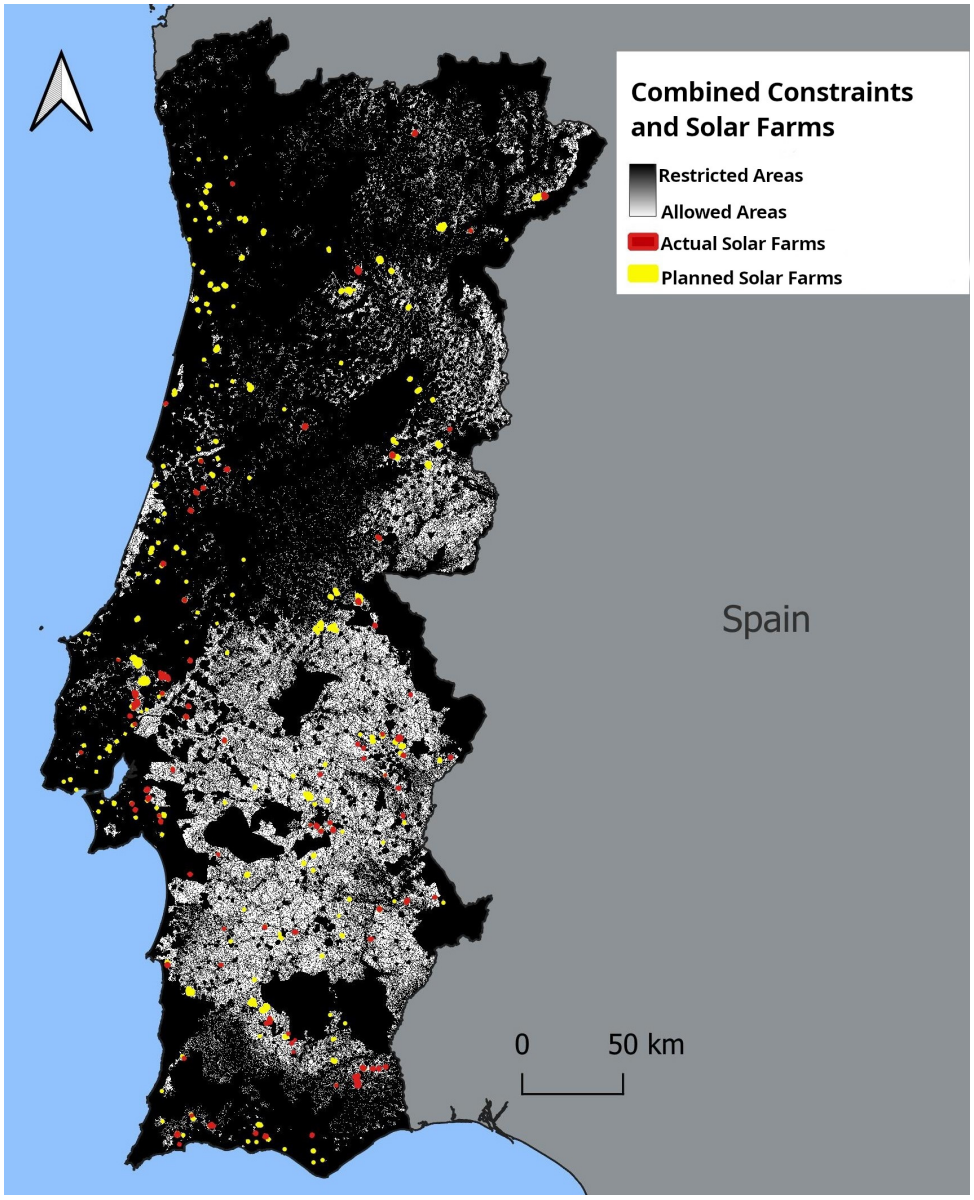

Figure 5.1: Combined Constraints Map: A composite map of applied restriction masks

5.2. Mapping the Suitability for PVF Deployment in Portugal

Based on the established evaluation criteria and applying the AHP methodology, a Land Suitability Map for PVFs in mainland Portugal was generated (Figure 5.2). This map spatially represents the Land Suitability Index (LSI), classifying viable areas for PVF installation into four categories: low suitability, moderate, suitable, and highly suitable, As shown in Section 4.1.4.

The results indicate that approximately:

- **1.80%** (1,603.42 km²) of the territory is highly suitable for PVFs (4);
- **12.73%** (11,328.91 km²) is considered suitable (3);

- **4.46%** (3,972.28 km²) presents moderate suitability (2);
- **0.05 km²%** (43.08 km²) is classified as having low suitability for PVFs (1).

Figure 5.2 shows that the highly suitable areas (represented in darker green) are concentrated mainly in the southern and inland regions of the country, where solar radiation is higher, slopes are favorable, and proximity to electrical infrastructure is greater. In contrast, areas classified as moderately or poorly suitable are found in regions with lower solar potential, environmental restrictions, or accessibility and infrastructure challenges.

Additionally, the Alentejo and Ribatejo regions stand out as strategic zones for PVF deployment due to the favorable combination of environmental, logistical, and territorial factors. These results reinforce the great potential of photovoltaic solar energy in Portugal and provide an objective basis for strategic decision-making and future expansion.

It is important to emphasize that the results of this study depend directly on the selected criteria and the weights assigned to them. Therefore, the model's suitability must consider the particularities of Portuguese territory and the priorities defined by regulatory bodies and energy sector stakeholders. In this study, the criteria were defined based on current European-Spanish legislation, scientific literature, and the analysis of available geospatial data, ensuring an integrated and evidence-based approach to solar farm planning in Portugal.

To assess the spatial distribution of land suitability for PVFs, a zonal analysis was performed using the final classified suitability raster. The raster has a spatial resolution of 25 m, so each pixel corresponds to 625 m². Using the «zonal-stats» function from the «rasterstats» package, we aggregated the number of pixels per suitability class within each administrative unit and calculated the corresponding area in square kilometers. Figure 5.3 complements the national suitability map by presenting an aggregated municipality-level view of suitable areas. The classification groups municipalities based on the extent of their land falling into higher suitability categories. This analysis helps highlight key regions for strategic investment. As expected, the southern and eastern municipalities, particularly in Alentejo and Ribatejo, stand out with the highest availability of optimal land for solar farm development, which reinforces the findings from the earlier national-scale AHP model.

To further quantify this pattern, we computed the area distribution of each suitability class at the district level (Figure 5.4). The districts of Évora and Beja dominate in terms of total land classified in excellent and high suitability categories, followed by Portalegre,

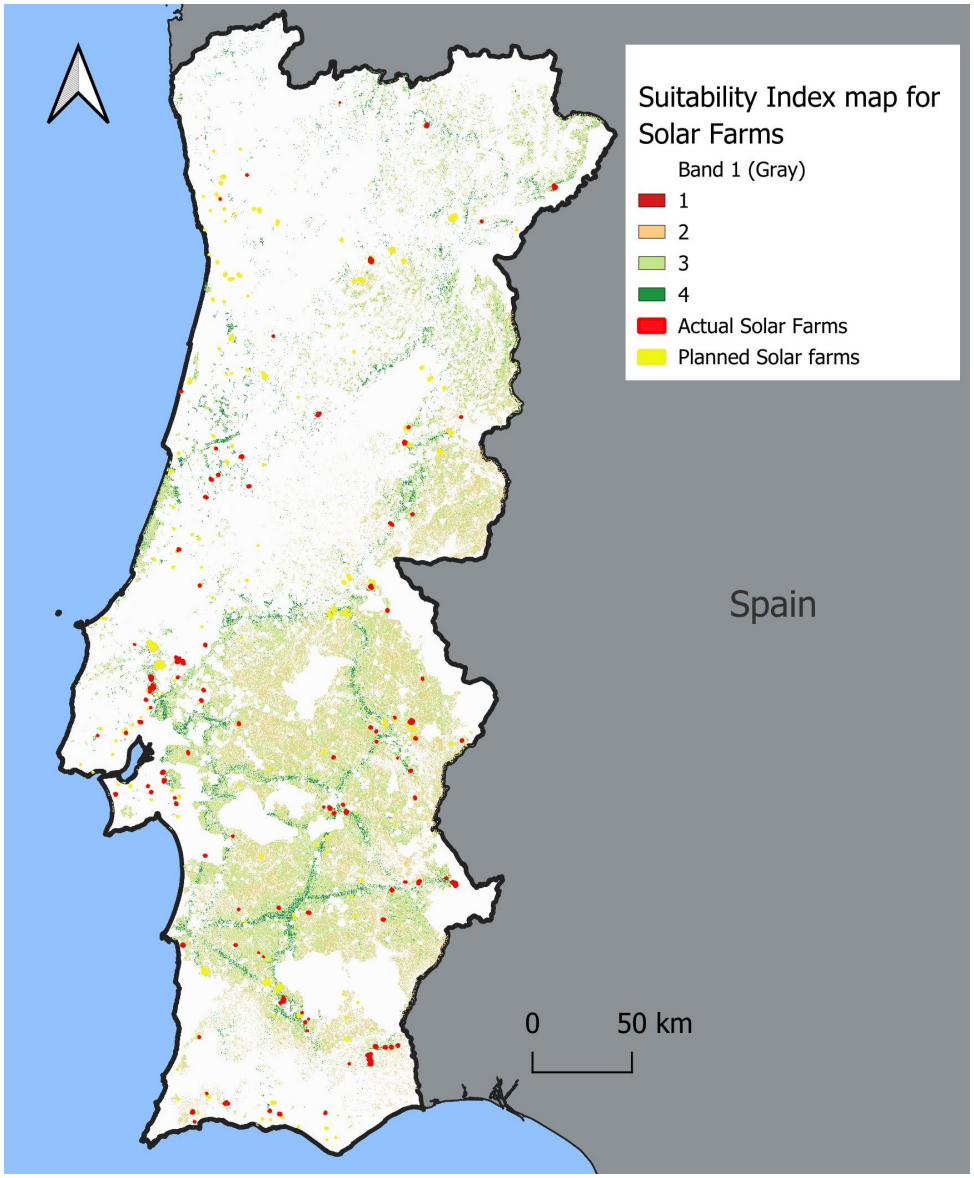

Figure 5.2: Spatial Suitability map for Photovoltaic Farm (PVF) installation

Setúbal, and Santarém. Across the entire country, 12 municipalities are classified as having excellent suitability, 28 as highly suitable, and 48 as moderately suitable, while the remaining municipalities fall into the low suitability category. This confirms that the most promising opportunities for solar development are highly concentrated, particularly in the southern half of Portugal, where environmental and infrastructural conditions favor large-scale photovoltaic deployment.

Drilling down into regional insights, we focused on the district of Évora due to its leading position in the national suitability rankings, see Figure 5.4. As one of the districts with the highest concentration of suitable land for photovoltaic deployment, it presents a valuable case study for finer-scale analysis. Accordingly, we performed the same classification

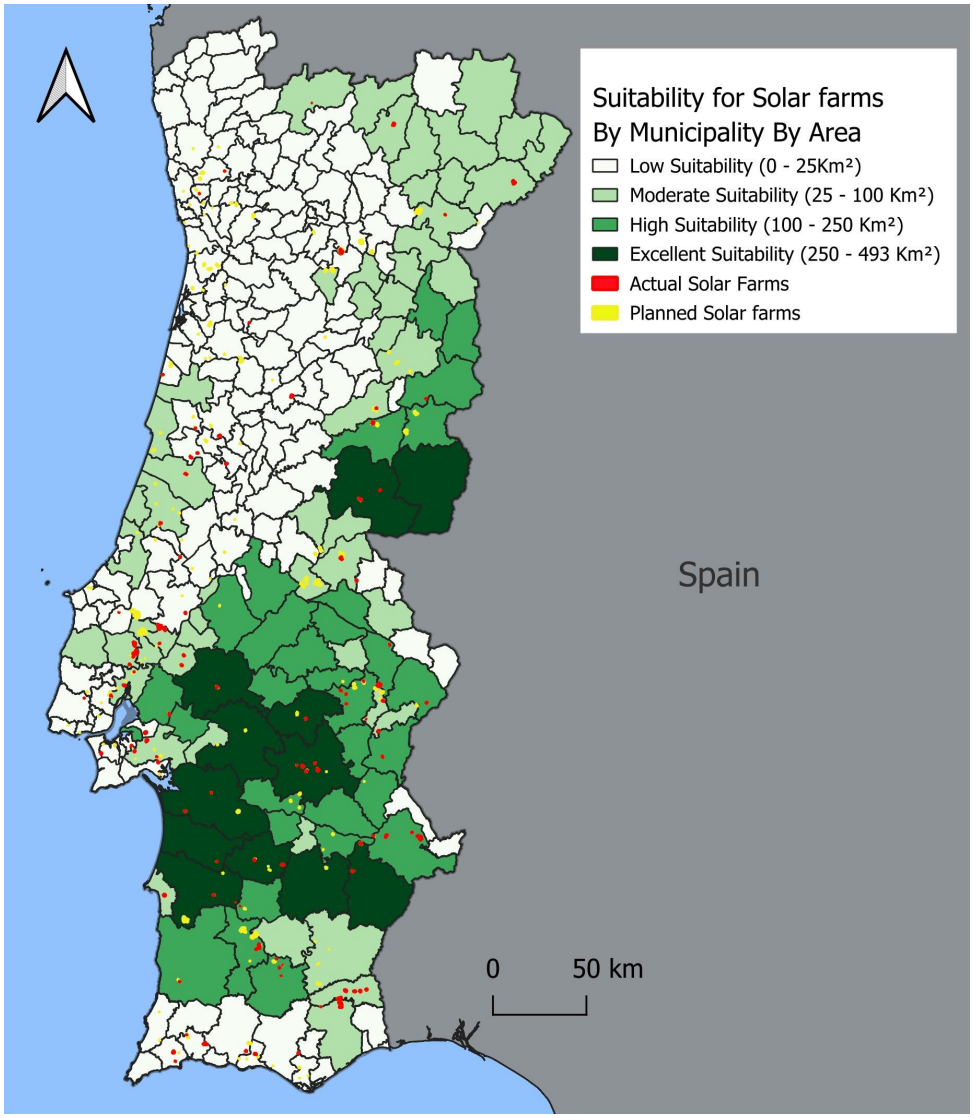

Figure 5.3: Spacial Suitability map for PVF installation by municipality with the actual and planned solar farms distribution

aggregation at the municipality (concelho) level within Évora, as shown in Figure 5.5. Municipalities such as Évora, Montemor-o-Novo, and Arraiolos exhibit the largest areas of land classified under the highest suitability classes (3 and 4), reinforcing the district's strategic relevance for solar farm planning and confirming its alignment with the suitability model's predictions.

To summarize the national landscape, we ranked all Portuguese municipalities by their total area in suitability indices 3 (suitable) and 4 (highly suitable). The top 20 municipalities Figure 5.6 show that Évora leads with nearly 493 km² of suitable land, followed by Santiago do Cacém, Montemor-o-Novo, and Serpa, each exceeding 370 km². This ranking also reveals a stark contrast across the country: while rural southern municipalities show high potential, many northern municipalities like Porto register no suitable area.

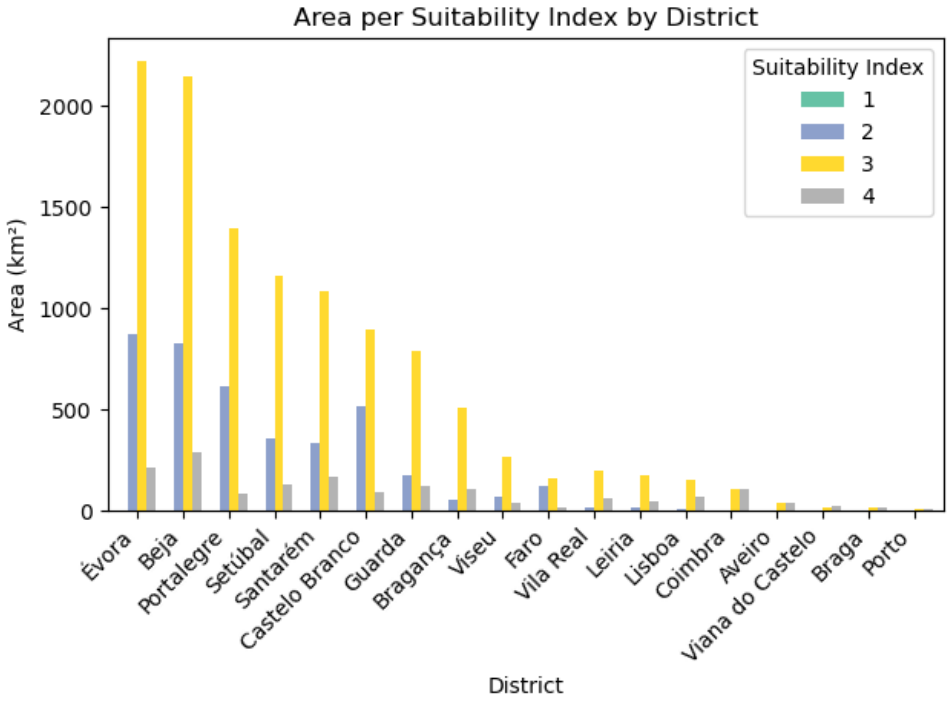

Figure 5.4: Distribution of Suitable Area for PVFs by District. 1: low suitability, 2: moderate suitability, 3: suitable 4: high suitability

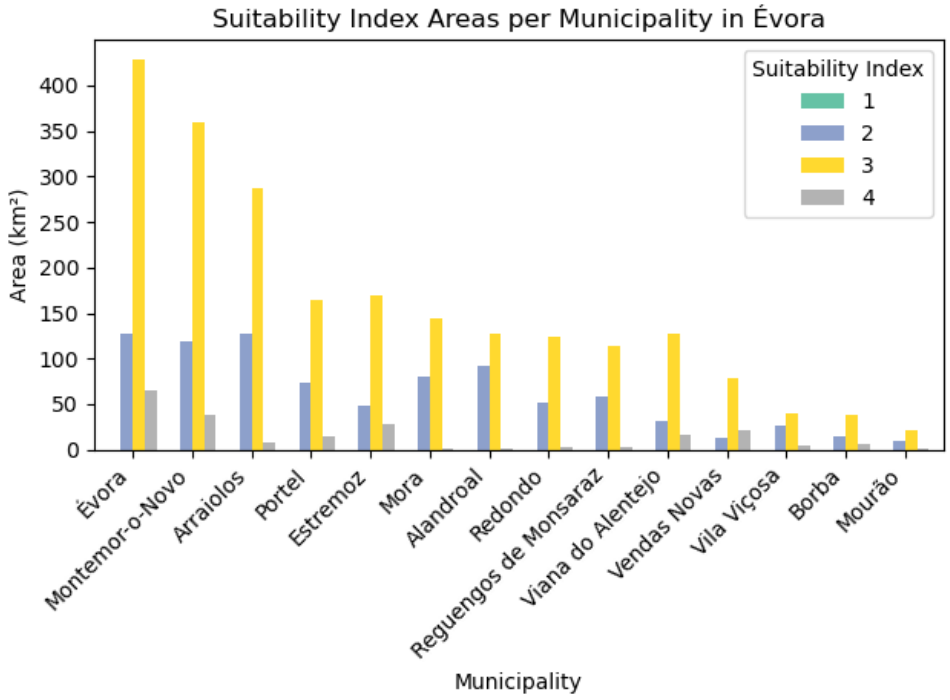

Figure 5.5: Suitability Index Distribution by Municipality within the District of Évora. 1: low suitability, 2: moderate suitability, 3: suitable 4: high suitability

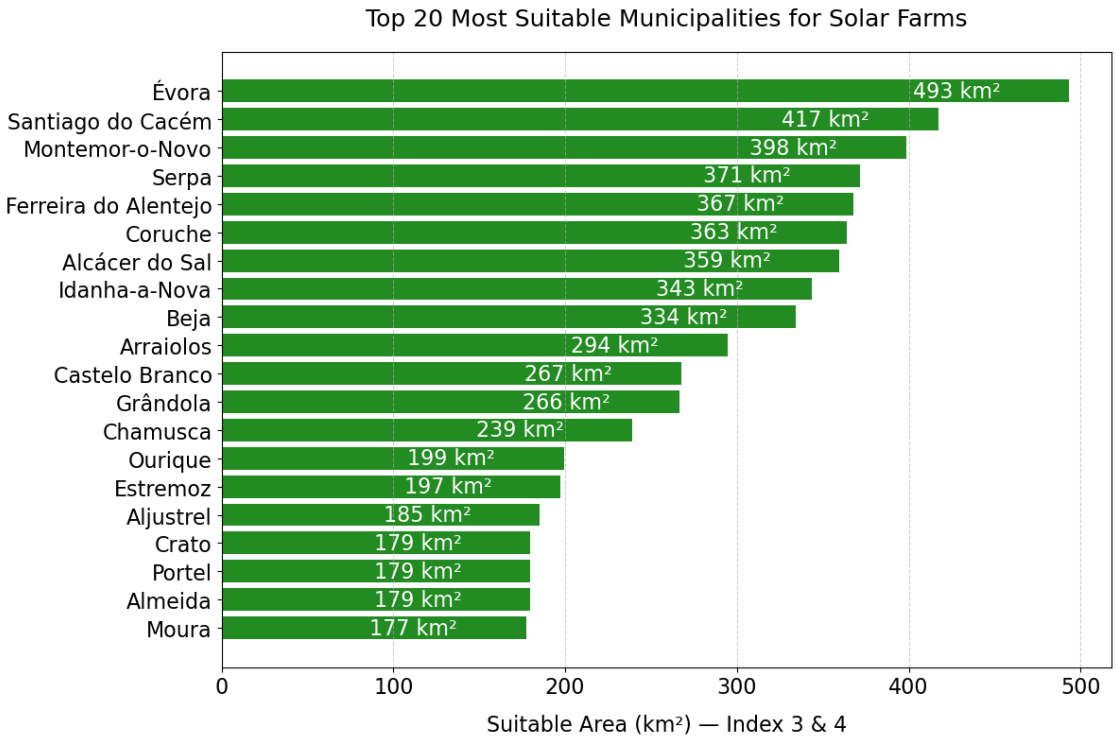

Figure 5.6: Top 20 municipalities in mainland Portugal with the largest area classified as highly or excellently suitable (classes 3 and 4) for PVF installation.

5.3. Evaluation of the actual and planned PVFs.

To assess the spatial coherence of solar farm placement, the distribution of actual and planned PVFs was overlaid on three key cartographic products: the combined constraint map (Figure 5.1), the overall suitability map (Figure 5.2), and the suitability classification aggregated by municipality (Figure 5.3). A visual inspection reveals that although a considerable number of solar farms, both existing and planned, coincide with areas identified as suitable, a significant portion still lies within poorly suitable or even restricted zones.

This section aims to quantitatively evaluate the spatial distribution of PVFs across two main dimensions: (1) restricted versus non-restricted areas, and (2) suitability classes within the non-restricted zones. The analysis is carried out under both the strict and moderate restriction scenarios, allowing a comparative understanding of how constraint severity affects the alignment between solar development and spatial planning criteria.

5.3.1 Distribution of Actual and Planned Solar Farms in Restricted Zones

To evaluate whether actual and planned PVFs comply with established land-use restrictions, two distinct scenarios were considered: a Strict Restriction Scenario and a Moderate Restriction Scenario. In both cases, spatial overlay analyses were performed using

binary masks representing restricted zones.

5.3.1.1 Strict Restriction Scenario

In the strict scenario, a conservative approach was applied where only areas fully free of any restriction were considered valid for solar development, applying the Strict Restriction Mask that combines all ten restriction criteria.

The results, summarized in Table 5.1, reveal that a considerable share of both actual and planned PVFs overlap with restricted areas. Specifically, **56.9%** of the actual and **55.8%** of the planned solar farm areas fall within strictly restricted zones. This indicates a significant misalignment between solar energy deployment and optimal site selection practices under strict regulatory compliance.

Table 5.1: Area of actual and planned photovoltaic farms overlapping restricted zones -Strict Scenario.

Restriction Type	PVF Type	Allowed (km²)	Restricted (km²)	Total (km²)	% in Restricted
Strict Combined	Actual	20.82	27.45	48.27	**56.9%**
Restrictions	Planned	40.47	51.05	91.52	**55.8%**

5.3.1.2 Moderate Restriction Scenario

A more flexible scenario was developed by combining six individual restriction layers: Special protected zones (CR1), National patrimony (CR7), Water bodies (CR2), Sensitive installations (CR10), Population clusters (CR8), and a 100-meter buffer around roads and railways (CR6). These layers were merged into a composite **Moderate Restriction Mask**, allowing a less stringent interpretation of constraints. Table 5.2 summarizes the results.

Table 5.2: Area of actual and planned PVFs overlapping restricted zones -Moderate Scenario.

Restriction Type	PVF Type	Allowed (km²)	Restricted (km²)	Total (km²)	% in Restricted
Moderate Combined Restrictions	Actual	32.34	15.93	48.27	**33.0%**
	Planned	66.45	25.07	91.52	**27.4%**
Special protected zones (CR1)	Actual	45.86	2.41	48.27	5.0%
	Planned	91.08	0.43	91.52	0.5%
National Patrimony (CR7)	Actual	48.26	0.01	48.27	0.02%
	Planned	91.01	0.51	91.52	0.6%
Water Bodies (CR2)	Actual	48.03	0.24	48.27	0.5%
	Planned	91.48	0.04	91.52	0.04%
Sensitive Installations (CR10)	Actual	46.76	1.51	48.27	3.1%
	Planned	87.72	3.80	91.52	4.2%
Population Clusters (CR8)	Actual	36.24	12.03	48.27	24.9%
	Planned	72.60	18.92	91.52	20.7%
Principal Roads (CR6)	Actual	46.88	1.39	48.27	2.9%
	Planned	86.34	5.17	91.52	5.6%

The results show that the Moderate Combined restriction—representing the union of all six individual masks—results in the largest overlaps: **33.0%** of the actual PVFs area and **27.4%** of the planned PVFs area fall within restricted zones. These values are significantly higher than those from any single restriction layer, which is expected since the composite mask captures all pixels that fall within any of the individual restricted categories.

It is important to note that the individual percentages do not sum up to the combined percentage. This is because the restricted areas are not mutually exclusive: a given pixel can simultaneously fall within multiple restriction types (e.g., near both a water body and a population cluster), but is only counted once in the combined mask. Thus, the composite result represents the union of overlapping restricted zones, not the arithmetic sum of individual overlaps.

From a policy and planning perspective, **population clusters** emerge as the most impactful single constraint, affecting nearly **25%** of the actual and **21%** of the planned solar

farm areas. In contrast, zones such as national patrimony and water bodies represent minimal overlaps. These findings underscore the importance of incorporating territorial constraints early in the planning process to enhance regulatory compliance, environmental sustainability, and public acceptance of solar energy development.

Further insights into the spatial distribution of solar farms within restricted zones are provided in Figure 5.7, which highlights the top 10 municipalities where actual and planned PVFs overlap with areas defined by the Moderate Combined restriction mask. Notably, municipalities such as Santarém, Rio Maior, and Ourique exhibit significant overlaps, with several square kilometers of solar installations located in zones that are environmentally or legally constrained. These results underscore the critical importance of incorporating spatial restriction layers during the early phases of solar energy planning, as they help prevent land-use conflicts and ensure compliance with conservation and zoning regulations.

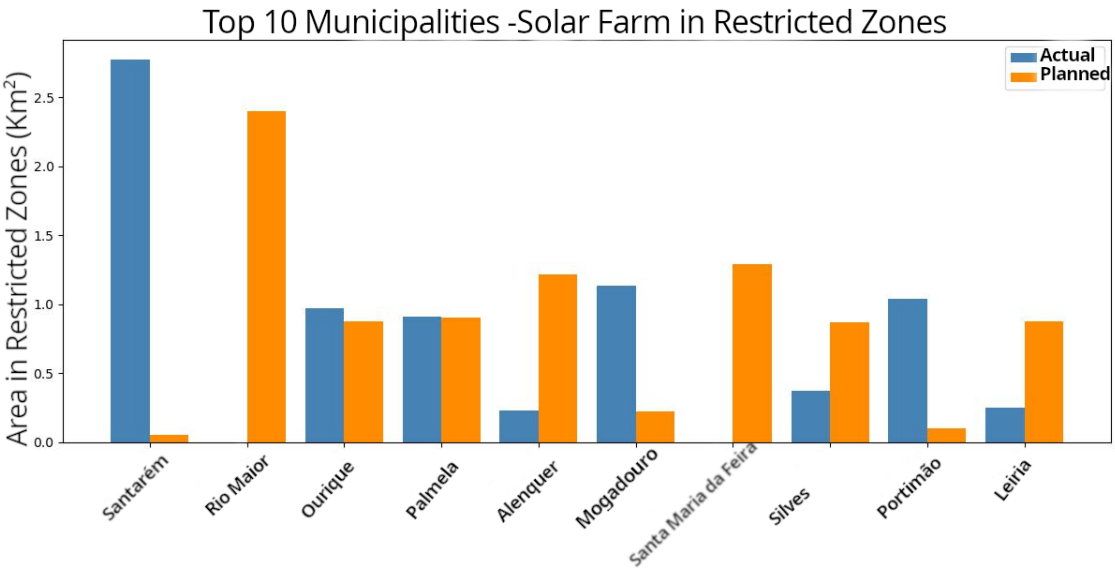

Figure 5.7: Top 10 municipalities with solar farms in Moderate Restriction areas

5.3.2 Distribution of Actual and Planned PVFs in Suitability Classes

While the previous section evaluated photovoltaic farms concerning restricted zones, the analysis now shifts focus toward suitability-based planning. This perspective not only identifies areas free from constraints but also evaluates their potential for solar development based on a range of economic and environmental factors. By comparing the spatial distribution of actual and planned solar farms against the derived suitability map, it becomes possible to assess whether site selection practices align with optimal conditions.

This provides a forward-looking tool for guiding the sustainable expansion of solar infrastructure across the territory.

Following the assessment that revealed a significant portion of both actual and planned solar farms are located in environmentally or legally restricted zones as high as 33% and 27.4%, respectively, under the moderate restriction mask, and 57% and 56%, respectively, under the Strict restriction mask, it becomes crucial to examine how these installations align with areas deemed suitable for photovoltaic deployment. To this end, we overlaid the solar farm raster layers on the reclassified AHP-based suitability map, which was generated by applying a strict restriction mask that combines all ten restriction criteria: Special protected zones, national patrimony, water bodies, extreme temperature, altitude, slope and aspect, sensitive installations, proximity to railways, principal roads and population clusters.

5.3.2.1 Strict Restriction Scenario

This approach ensures that only land parcels completely free from restrictions are evaluated for suitability. As a consequence of this strict scenario, a significant portion of both actual and planned solar farms overlaps with restricted zones, which are therefore excluded from the suitability classification. The low suitability class (1) is absent from the results, not due to the masking process, but rather because no actual or planned solar farm pixels were located in areas classified with this low suitability level. The moderate suitability (2) is also negligible.

Table 5.3 presents the distribution of actual and planned solar farm areas suitability classes under this strict scenario. Over **55%** of the total installed or planned PV area falls outside classified zones due to their location within restricted regions. Among classified areas, the suitable class (3) dominates, indicating that while unsuitable locations are largely avoided, there is no consistent prioritization of the most suitable available land (class 4).

Table 5.3: Distribution of actual and planned SFs areas across suitability classes (AHP map with strict restriction mask)

Suitability Class	Solar Farm Type	Area (km^2)	% of Solar Area
Moderate suitability (2)	Actual	2.46	5.1%
	Planned	4.75	5.2%
Suitable (3)	Actual	13.80	28.6%
	Planned	28.72	31.4%
Highly suitable (4)	Actual	4.56	9.4%
	Planned	7.00	7.6%
Restricted	Actual	27.45	56.9%
	Planned	51.05	55.8%

5.3.2.2 Moderate Restriction Scenario

To provide a more inclusive view, the analysis was repeated using the moderate restriction mask, which allows evaluation of a larger land base. This reveals a richer distribution of suitability classes, including the appearance of class 1 (very low suitability), albeit with negligible planned PVFs overlap.

As shown in Table 5.4, the majority of actual and planned solar farms still occupy areas classified as **suitable class (3)**, accounting for **41.1%** and **48.1%**, respectively. Importantly, the proportion of PVFs in restricted areas drops significantly, reflecting the wider extent of classified land. This highlights how planning constraints directly shape the usable area and, consequently, the suitability assessment.

Table 5.4: Distribution of actual and planned solar farm areas across suitability classes (AHP map with moderate restriction mask)

Suitability Class	Solar Farm Type	Area (km^2)	% of Solar Area
Very Low Suitability (1)	Actual	0.00	0.0%
	Planned	0.01	0.0%
Moderate Suitability (2)	Actual	5.32	11.0%
	Planned	11.58	12.7%
Suitable (3)	Actual	19.86	41.1%
	Planned	44.06	48.1%
Highly Suitable (4)	Actual	7.15	14.8%
	Planned	10.80	11.8%
Restricted	Actual	15.93	33.0%
	Planned	25.07	27.4%

5.4. Discussion

The findings of this study affirm that only 19% of mainland Portuguese territory meets the criteria for PVF development, with up to 15% classified as suitable to highly suitable. These suitable lands are predominantly concentrated in the southern and inland regions, with the Alentejo and Ribatejo regions standing out as strategic zones for PVF deployment due to their favorable combination of solar potential, logistical accessibility, and land availability. At the district level, Évora ranks at the top, offering more than 2000 km² of land classified as suitable or highly suitable. Within this district, the Évora municipality emerges as the most optimal, with approximately 500 km² of high-quality land for solar development. Nationwide, 12 municipalities are classified as having excellent suitability, 28 as highly suitable, and 48 as moderately suitable, while the rest fall into the low suitability category. This distribution highlights that the most promising opportunities for solar energy expansion are geographically concentrated, particularly in the southern half of Portugal, where environmental and infrastructural conditions align to support large-scale photovoltaic deployment.

This observation aligns with the national-scale study by This observation aligns with the national-scale study by [19], which remains the only other comprehensive photovoltaic suitability assessment covering mainland Portugal. Their methodology employed a GIS-based MCDM framework using the TOPSIS. In this approach, each municipality was treated as an alternative and evaluated against a set of standardized criteria, including

GHI, PVOUT, municipality size, distances from touristic zones and coastline, distance from protected areas, and distance from forests, agriculture, and tree plantations. All criteria were assigned equal weight. There is no restriction criterion here, only classification. The process involved constructing a normalized decision matrix, computing distances from ideal and anti-ideal solutions, and calculating a Suitability Index (SI) for each municipality. Municipalities were then ranked based on their SI scores. In the last phase, focused on Mértola—ranked highest in their suitability index- they integrated a full set of constraints and classification criteria.

However, this research departs methodologically in key aspects. While Spyridonidou *et al.* [19] applied no exclusion framework, our study adopted a first restrictive phase and context-sensitive approach. We incorporated ten exclusion layers representing biophysical, infrastructural, and socio-environmental constraints—including Natura 2000 zones, water bodies, terrain slope and aspect, and population density buffers. As a result, the proportion of land classified as suitable was significantly reduced.

Interestingly, both studies identified 12 municipalities as falling within the highest suitability class (Figure 5.8, Figure 5.3). However, a notable misalignment exists in the composition of these top-ranked municipalities: several municipalities classified as having excellent suitability in the study by Spyridonidou et al. [19] are considered only moderately suitable in our analysis. This divergence is particularly evident in the case of Bragança, which in our model does not meet the necessary energetic and infrastructural conditions to warrant the highest suitability classification. Specifically, Bragança exhibits low solar irradiance and practical PVOUT values (Figures 3.11, 3.12), extreme altitude conditions (Figure 3.3), high inclination and unfavorably oriented terrain (Figure 3.4), low long-term average temperature (Figure 3.9), and lack of proximity to high-voltage grid infrastructure (Figure 3.14). These factors collectively lower its suitability score under our stricter, context-sensitive model.

This methodological divergence underscores the critical influence of exclusion criteria application and weight allocation on final suitability outcomes. It also explains why our results contrast with the broader suitability classifications observed by Spyridonidou et al. [19], where 274 municipalities were considered excellent or highly suitable, under more relaxed assumptions based on only classification. Their analysis did not include a preliminary restriction phase to exclude environmentally or technically incompatible areas. Instead, all spatial criteria were treated uniformly, where factors such as proximity to touristic zones,

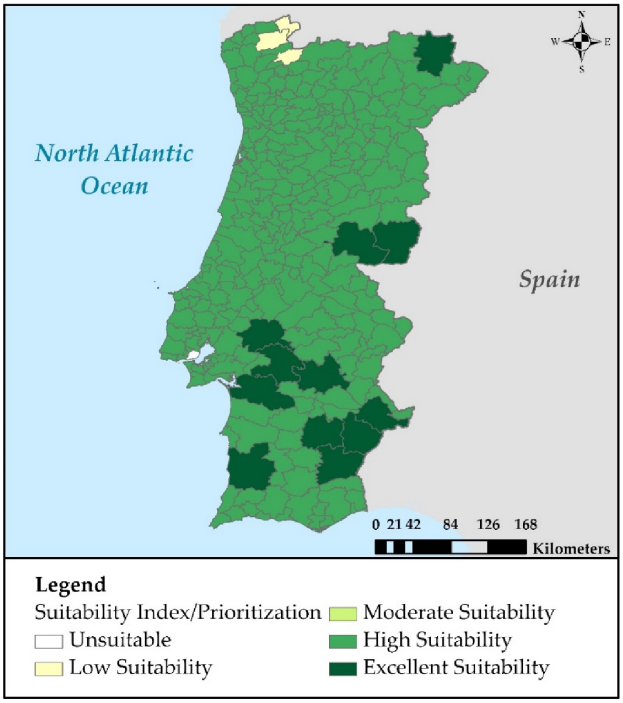

Figure 5.8: Prioritization results of the municipalities of the Portuguese mainland by Spyridonidou et al. [19]

location within protected areas, or even low GHI and PVOUT values were considered as equally important classification variables. This likely led to an overestimation of suitability in several areas that, under a more restrictive and differentiated framework like ours, would not qualify as viable for photovoltaic development.

While the subjectivity of pairwise comparisons is often cited as a limitation, this is in fact the core strength of AHP in real-world planning contexts: it allows for flexible integration of expert knowledge, legal frameworks, and policy priorities. In this context, the importance of criteria is not arbitrarily assumed but rather informed by domain-specific knowledge. For instance, Global Horizontal Irradiance GHI, a key factor in solar energy generation, should carry significantly more weight than criteria such as slope or aspect, which can often be mitigated through engineering adaptations. Assigning equal weights to all criteria would ignore these physical and economic realities and lead to unrealistic suitability outcomes.

Although some literature includes TOPSIS [19] or fuzzy extensions to AHP that address uncertainty in human judgment [72], the classical AHP framework was adopted here due to its clarity, interpretability, and direct alignment with expert-informed decision-making processes applicable in territorial planning and renewable energy site selection.

A key contribution of this work lies in the inclusion of a dedicated evaluation phase, which assesses the spatial distribution of both existing and planned PVF installations against

a binary restriction map and a suitability classification, under two distinct scenarios: strict and moderate. This integration of real-world deployment data provides critical insight into whether current decision-making strategies align with biophysical, environmental, and technical criteria. Where misalignment is identified, the framework offers a valuable tool for reassessing and improving national siting strategies to better reflect scientifically grounded priorities. Our overlay analysis confirmed that, even under more lenient planning assumptions, a significant portion of PVF, under strict restriction scenarios, more than half of existing or planned solar farms are situated in constrained zones, additionally PVF development in Portugal continues to take place in suboptimal suitable zones. This spatial misalignment highlights the urgent need for more robust planning frameworks that prioritize ecological integrity and regulatory compliance.

Our findings also reinforce concerns raised by national regulatory bodies. The Comissão de Avaliação (2021) [73] cautioned against the growing concentration of solar farms in ecologically sensitive areas, urging improved spatial equity and environmental oversight.

These patterns are not unique to Portugal. Comparative analysis with recent studies in Spain, particularly those examining the Jimena Depression in Andalusia [4], reveals parallel challenges. In both countries, more than 20% of solar development occurs in protected or unsuitable areas, driven by land availability and grid access pressures. These shared experiences underscore the broader need for integrative planning frameworks that reconcile energy policy with ecological and social realities.

Overall, this study contributes to an evolving body of international research advocating for spatially explicit, environmentally grounded solar energy strategies. By applying a stricter and more nuanced evaluation at a national scale, we highlight the necessity of moving beyond technical feasibility toward a balanced approach that integrates ecological protection, spatial justice, and long-term sustainability.

5.4.1 Complementary Deep Learning Model for Solar Farm Detection

Beyond the spatial suitability framework presented herein, a complementary solar farm detection model, **Detect-solar**, was developed as an experimental side-project. This model uses high-resolution GEOSAT-2 imagery to detect solar farms. GEOSAT-2 is a very high-resolution Earth observation satellite that carries a push-broom camera with one panchromatic band (PAN, 0.75 m resolution) and four multispectral bands (R, G, B, NIR at 4 m resolution). The images used in this study were pan-sharpened to **1m** resolution and are ortho-rectified with geolocation errors generally below 4 meters when compared to the national orthophotomap DGT [74], which is negligible for the intended application. CEiiA is actively involved in the operation and ground segment of GEOSAT-2, contributing to the availability of this imagery for national and European projects.

The dataset was composed of 256x256 tiles combining RGB, NIR, and derived spectral and texture indices. A U-Net architecture with a ResNet34 backbone was trained on manually annotated solar farm tiles. The Figure 5.9 shows the full processing pipeline of the Detect-solar model.

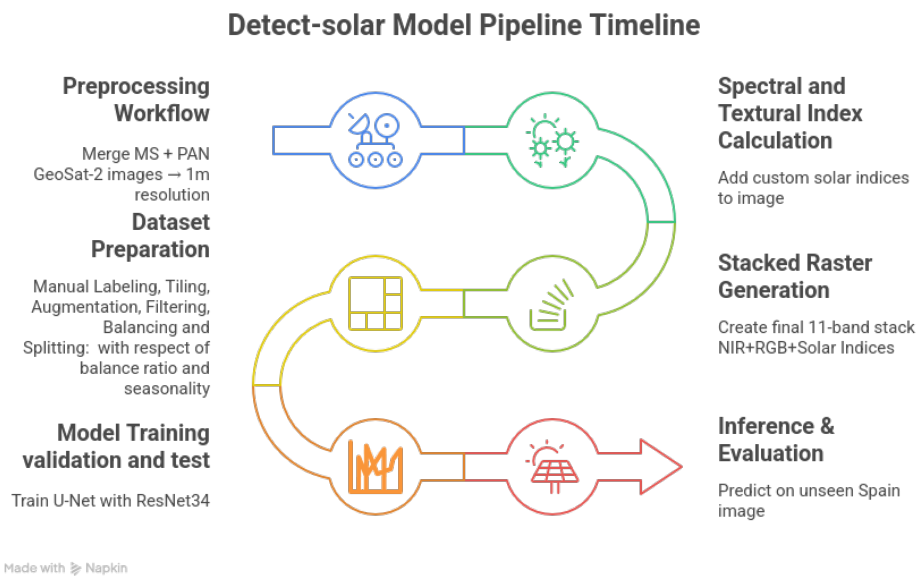

Figure 5.9: Flowchart of Detect-Solar Model.

The preliminary results of the deep learning model Detect-Solar demonstrated promising performance, achieving an F1-score of 0.96. As illustrated in Figure 5.10, the model accurately inferred the presence of solar infrastructure in an unseen GEOSAT-2 image from Spain. Although this model was not part of the core methodology of the present dissertation, it serves as a proof of concept for the future integration of deep learning techniques

into national workflows for solar infrastructure mapping and inventory validation. This automated approach highlights the potential of leveraging AI-based tools to support real-time detection and monitoring of photovoltaic installations across Portugal, contributing to a more efficient and scalable renewable energy planning system.

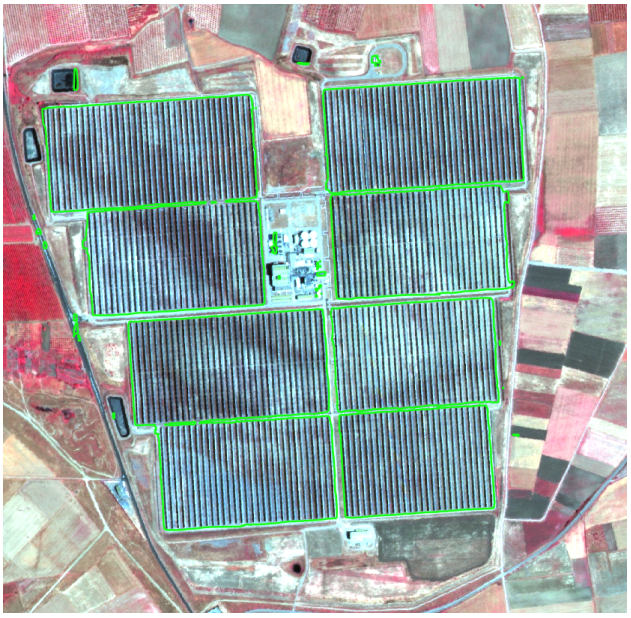

Figure 5.10: Detect-solar Predictions of Consoll Orellana PVF (Spain)

6. Conclusions

This study proposed and implemented a geospatial methodology for identifying optimal sites for the installation of PVFs in mainland Portugal. Through an integrated GIS and MCDM approach, particularly employing the AHP, we developed both national and municipal-level suitability maps and evaluated the spatial alignment of actual and planned solar farms with these suitability assessments.

Summary of Key Findings

- A total of ten restriction criteria—covering environmental, infrastructural, and socio-spatial constraints—were defined and combined into strict and moderate exclusion masks to identify areas unsuitable for PVFs deployment. As a result, approximately 70% of mainland Portugal was classified as infeasible for photovoltaic development under current regulatory and ecological constraints.

- Based on the AHP-weighted criteria and subcriteria, a national suitability map was generated for the remaining unrestricted areas. Suitability scores were then classified into four categories: low, moderate, suitable, and highly suitable.

- The analysis shows that only **1.80%** of mainland Portugal is classified as highly suitable for PVF installation, while approximately **12.7%** is considered suitable. These areas are concentrated mostly in southern and inland districts, particularly in the Alentejo region.

- Municipal-level analysis identified districts like Évora, Montemor-o-Novo, Serpa, and Santiago do Cacém as having the largest highly suitable surfaces and the highest concentration of PVF installations.

- A significant proportion of **actual** (57%) and **planned** (56%) solar farms are located in restricted zones when evaluated using the strict exclusion mask. Even under the moderate scenario, **33%** of actual and **27.4%** of planned PVFs overlap with areas where development is environmentally or legally discouraged.

- The spatial analysis revealed that most existing and planned PVF installations are located in moderately suitable areas, with only a small share occupying highly suitable zones. Among the restriction types, population clusters and proximity to

sensitive infrastructure were the most frequently infringed constraints, while protected areas and heritage zones showed fewer conflicts. These patterns suggest that non-technical factors—such as land availability, administrative ease, or grid access—play a decisive role in current siting decisions, often overriding optimal technical suitability.

Implications and Recommendations

- The results emphasize the urgent need to align solar energy planning with ecological and regulatory constraints. Overlaying PVFs siting decisions with restriction masks in the early planning stages could help prevent land-use conflicts and environmental degradation.
- The mismatch between technical suitability and actual/planned PVFs locations suggests the importance of integrating socio-political and economic layers (e.g., land price, ownership) in future multi-criteria models.
- Municipal and regional decision-makers could benefit from adopting this methodology for proactive spatial planning, prioritizing areas where investment is both technically viable and environmentally sustainable.
- Future studies should incorporate temporal dynamics (e.g., seasonal irradiance) and monitor post-installation impacts on landscape and biodiversity to ensure truly sustainable development.
- The integration of AI-based tools like the **Detect-Solar** model—capable of automatically identifying solar farms from high-resolution satellite imagery—offers promising potential for real-time monitoring, inventory validation, and support to national agencies in ensuring compliance with spatial regulations.

Final Remarks

This study proposed a reproducible and scalable geospatial methodology for identifying suitable locations for PVFs in mainland Portugal. By combining exclusion rules grounded in legal, environmental, and infrastructural constraints with a weighted AHP-based classification model, the framework bridges technical rigor with real-world planning challenges.

The spatial overlay analysis revealed a persistent misalignment between scientific recommendations and actual deployment patterns: a significant share of existing and planned

PVFs are situated in restricted or suboptimal areas, even under moderate planning assumptions. These findings support recent concerns raised by national authorities, such as the Comissão de Avaliação Interministerial (2021) [73], and emphasize the need for spatially informed, regulation-compliant planning tools.

To complement this strategic perspective, a deep learning model—**Detect-Solar**—was also developed as a proof-of-concept for automated detection of solar farms from high-resolution GEOSAT-2 imagery. This contribution highlights the potential of AI-based monitoring solutions to support inventory updates, enforcement efforts, and national-scale tracking of PVF deployment.

Together, these components provide a robust foundation for guiding solar energy expansion in Portugal, ensuring that sustainability targets are met not only in energy output but also in environmental stewardship and territorial equity.

References

[1] Nações Unidas. (2024, Dec.) Onu alerta que 2024 pode terminar como o ano mais quente da história. [Online]. Accessed: 27-Jun-2025. [Online]. Available: https://news.un.org/pt/story/2024/12/1842841 [Cited on page 1.]

[2] NOAA National Centers for Environmental Information. (2025, Jan.) Global climate report - january 2025. [Online]. Accessed: 27-Jun-2025. [Online]. Available: https://www.ncei.noaa.gov/access/monitoring/monthly-report/global/202501 [Cited on page 1.]

[3] European Commission. (2024) Less developed regions hold the key for europe's energy transition. [Online]. Accessed: 27-Jun-2025. [Online]. Available: https: //cohesiondata.ec.europa.eu/stories/s/ucma-sjp3 [Cited on page 1.]

[4] C. López-Bravo, L. Mora-López, M. Sidrach-deCardona, and M. J. Márquez-Ballesteros, "A comprehensive analysis based on GIS-AHP to minimise the social and environmental impact of the installation of large-scale photovoltaic plants in south Spain," *Renewable Energy*, vol. 226, p. 120387, May 2024. [Online]. Available: https://linkinghub.elsevier.com/retrieve/pii/S096014812400452X [Cited on pages 1, 3, 7, 19, 26, and 59.]

[5] X. García-Casals, R. Ferroukhi, and B. Parajuli, "Measuring the socio-economic footprint of the energy transition," *Energy Transitions*, vol. 3, pp. 105–118, 2019. [Online]. Available: https://doi.org/10.1007/s41825-019-00018-6 [Cited on page 2.]

[6] J. Arán Carrión, A. Espín Estrella, F. Aznar Dols, M. Zamorano Toro, M. Rodríguez, and A. Ramos Ridao, "Environmental decision-support systems for evaluating the carrying capacity of land areas: Optimal site selection for grid-connected photovoltaic power plants," *Renewable and Sustainable Energy Reviews*, vol. 12, no. 9, pp. 2358–2380, Dec. 2008. [Online]. Available: https://linkinghub.elsevier.com/retrieve/pii/S1364032107001049 [Cited on page 2.]

[7] C. Candelise, M. Winskel, and R. J. Gross, "The dynamics of solar pv costs and prices as a challenge for technology forecasting," *Renewable and Sustainable Energy Reviews*, vol. 26, pp. 96–107, October 2013. [Online]. Available: https://doi.org/10.1016/j.rser.2013.05.012 [Cited on page 2.]

[8] International Renewable Energy Agency (IRENA), “Renewable capacity statistics 2024,” International Renewable Energy Agency, Abu Dhabi, Tech. Rep., 2024, accessed: 2025-06-26. [Online]. Available: https://www.irena.org/-/media/Files/IRENA/Agency/Publication/2024/Mar/IRENA_RE_Capacity_Statistics_2024.pdf [Cited on page 2.]

[9] Energy Institute, “Statistical review of world energy 2024,” Energy Institute, London, Tech. Rep., 2024, accessed: 2025-06-26. [Online]. Available: https://www.energyinst.org/__data/assets/pdf_file/0006/1542714/684_EI_Stat_Review_V16_DIGITAL.pdf [Cited on page 2.]

[10] REN - Redes Energéticas Nacionais, “Integrated report 2024: Energy in balance – accelerate the future, preserve the present,” REN - Redes Energéticas Nacionais, Lisbon, Portugal, Tech. Rep., 2024, accessed: 2025-06-26. [Online]. Available: https://www.ren.pt/media/hkmms4rx/ren-integrated-report-2024.pdf [Cited on page 3.]

[11] “Regulamento (UE) 2024/223 do Conselho, de 22 de dezembro de 2023,” https://eur-lex.europa.eu/legal-content/PT/TXT/PDF/?uri=OJ:L:2024:002:FULL&from=PT, Dec. 2023, altera o Regulamento (UE) 2022/2577 que estabelece um regime para acelerar a implantação das energias renováveis. [Cited on page 3.]

[12] “Decreto-lei n.º 96/2017, de 10 de agosto,” https://dre.pt/dre/detalhe/decreto-lei/96-2017-107987277, pp. 4654–4663, Aug. 2017, estabelece o regime das instalações elétricas particulares. [Cited on page 3.]

[13] T. L. Saaty, “A scaling method for priorities in hierarchical structures,” *Journal of Mathematical Psychology*, vol. 15, no. 3, pp. 234–281, 1977. [Online]. Available: https://doi.org/10.1016/0022-2496(77)90033-5 [Cited on pages 4, 5, 30, 33, and 42.]

[14] H. Z. Al Garni and A. Awasthi, “Solar PV power plant site selection using a GIS-AHP based approach with application in Saudi Arabia,” *Applied Energy*, vol. 206, pp. 1225–1240, Nov. 2017. [Online]. Available: https://linkinghub.elsevier.com/retrieve/pii/S030626191731437X [Cited on pages 6 and 9.]

[15] A. Aly, S. S. Jensen, and A. B. Pedersen, “Solar power potential of Tanzania: Identifying CSP and PV hot spots through a GIS multicriteria decision making analysis,” *Renewable Energy*, vol. 113, pp. 159–175, Dec. 2017. [Online]. Available:

https://linkinghub.elsevier.com/retrieve/pii/S0960148117304718 [Cited on pages 6, 9, 10, 17, 18, and 19.]

[16] A. Asakereh, M. Soleymani, and M. J. Sheikhdavoodi, “A GIS-based Fuzzy-AHP method for the evaluation of solar farms locations: Case study in Khuzestan province, Iran,” *Solar Energy*, vol. 155, pp. 342–353, Oct. 2017. [Online]. Available: https://linkinghub.elsevier.com/retrieve/pii/S0038092X17304851 [Cited on pages 6 and 9.]

[17] A. Vrînceanu, M. Dumitraşcu, and G. Kucsicsa, “Site suitability for photovoltaic farms and current investment in Romania,” *Renewable Energy*, vol. 187, pp. 320–330, Mar. 2022. [Online]. Available: https://linkinghub.elsevier.com/retrieve/pii/S0960148122000970 [Cited on pages 6, 17, and 18.]

[18] S. Sindhu, V. Nehra, and S. Luthra, “Investigation of feasibility study of solar farms deployment using hybrid AHP-TOPSIS analysis: Case study of India,” *Renewable and Sustainable Energy Reviews*, vol. 73, pp. 496–511, Jun. 2017. [Online]. Available: https://linkinghub.elsevier.com/retrieve/pii/S1364032117301405 [Cited on pages 7 and 9.]

[19] S. Spyridonidou, E. Loukogeorgaki, D. G. Vagiona, and T. Bertrand, “Towards a Sustainable Spatial Planning Approach for PV Site Selection in Portugal,” *Energies*, vol. 15, no. 22, p. 8515, Jan. 2022, number: 22 Publisher: Multidisciplinary Digital Publishing Institute. [Online]. Available: https://www.mdpi.com/1996-1073/15/22/8515 [Cited on pages vi, 7, 9, 17, 18, 19, 56, 57, and 58.]

[20] O. N. Mensour, B. El Ghazzani, B. Hlimi, and A. Ihlal, “A geographical information system-based multi-criteria method for the evaluation of solar farms locations: A case study in Souss-Massa area, southern Morocco,” *Energy*, vol. 182, pp. 900–919, Sep. 2019. [Online]. Available: https://linkinghub.elsevier.com/retrieve/pii/S0360544219311946 [Cited on pages 7 and 9.]

[21] T. Finn and P. McKenzie, “A high-resolution suitability index for solar farm location in complex landscapes,” *Renewable Energy*, vol. 158, pp. 520–533, Oct. 2020. [Online]. Available: https://linkinghub.elsevier.com/retrieve/pii/S0960148120308259 [Cited on page 7.]

[22] M. Giamalaki and T. Tsoutsos, “Sustainable siting of solar power installations in Mediterranean using a GIS/AHP approach,” *Renewable Energy*, vol. 141, pp.

64–75, Oct. 2019. [Online]. Available: https://linkinghub.elsevier.com/retrieve/pii/S0960148119304124 [Cited on pages 8 and 9.]

[23] J. R. Janke, “Multicriteria GIS modeling of wind and solar farms in Colorado,” *Renewable Energy*, vol. 35, no. 10, pp. 2228–2234, Oct. 2010. [Online]. Available: https://linkinghub.elsevier.com/retrieve/pii/S096014811000131X [Cited on page 8.]

[24] A. M. Kowalczyk and S. Czyża, “Optimising Photovoltaic Farm Location Using a Capabilities Matrix and GIS,” *Energies*, vol. 15, no. 18, p. 6693, Sep. 2022. [Online]. Available: https://www.mdpi.com/1996-1073/15/18/6693 [Cited on page 8.]

[25] E. Tercan, A. Eymen, T. Urfalı, and B. O. Saracoglu, “A sustainable framework for spatial planning of photovoltaic solar farms using GIS and multi-criteria assessment approach in Central Anatolia, Turkey,” *Land Use Policy*, vol. 102, p. 105272, Mar. 2021. [Online]. Available: https://linkinghub.elsevier.com/retrieve/pii/S0264837720326107 [Cited on page 8.]

[26] N. Kranjčić, A. Bek, B. Đurin, S. K. Singh, and S. Kanga, “ANALYSIS OF SOLAR ENERGY POTENTIAL BY REMOTE SENSING TECHNIQUES IN VARAŽDINSKA COUNTY, CROATIA,” *The International Archives of the Photogrammetry, Remote Sensing and Spatial Information Sciences*, vol. XLVI-4/W5-2021, pp. 343–347, Dec. 2021. [Online]. Available: https://isprs-archives.copernicus.org/articles/XLVI-4-W5-2021/343/2021/ [Cited on page 8.]

[27] I. Potić, R. Golić, and T. Joksimović, “Analysis of insolation potential of Knjaževac Municipality (Serbia) using multi-criteria approach,” *Renewable and Sustainable Energy Reviews*, vol. 56, pp. 235–245, Apr. 2016. [Online]. Available: https://linkinghub.elsevier.com/retrieve/pii/S1364032115013234 [Cited on page 8.]

[28] D. Doljak and G. Stanojević, “Evaluation of natural conditions for site selection of ground-mounted photovoltaic power plants in Serbia,” *Energy*, vol. 127, pp. 291–300, May 2017. [Online]. Available: https://linkinghub.elsevier.com/retrieve/pii/S0360544217305339 [Cited on page 9.]

[29] B. Elboshy, M. Alwetaishi, R. M. H. Aly, and A. S. Zalhaf, “A suitability mapping for the PV solar farms in Egypt based on GIS-AHP to optimize multi-criteria feasibility,” *Ain Shams Engineering Journal*, vol. 13, no. 3, p. 101618, May 2022. [Online]. Available: https://linkinghub.elsevier.com/retrieve/pii/S209044792100383X [Cited on page 9.]

[30] Instituto Geográfico Português, *Atlas de Portugal*, R. S. de Brito, Ed. Lisboa: Instituto Geográfico Português, 2005, il. ; 32 cm. [Cited on page 12.]

[31] World Bank Group and ESMAP, "Global solar atlas," https://globalsolaratlas.info/map, 2025, version 2.12 released in April 2025. [Cited on pages 12, 13, 20, 22, and 23.]

[32] Copernicus Climate Change Service, "Climate indicators: Temperature," https://climate.copernicus.eu/climate-indicators/temperature, 2025, accessed: 2025-06-26. [Cited on pages 13 and 20.]

[33] Instituto Português do Mar e da Atmosfera (IPMA), "Portal ipma – instituto português do mar e da atmosfera," https://www.ipma.pt/pt/index.html, 2025, accessed: 2025-06-26. [Cited on pages 13 and 24.]

[34] Gonçalves, José Alberto, "Dem data for portugal," https://www.fc.up.pt/pessoas/jagoncal/dems/, 2025, accessed: 2025-06-26. [Cited on pages 13 and 17.]

[35] UNEP-WCMC and IUCN, "Protected planet: The world database on protected areas (wdpa)," https://www.protectedplanet.net/en, 2025, accessed: 2025-06-26. [Cited on pages 13 and 15.]

[36] Direção-Geral do Território, "SRUP - Rede Natura 2000 - Zonas de Proteção Especial," https://www.dgterritorio.gov.pt/dados-abertos, 2021, servidão e Restrição de Utilidade Pública (SRUP) relativa à Rede Natura 2000 em vigor em Portugal Continental. [Cited on pages 13 and 16.]

[37] ——, "Carta do Regime de Uso do Solo – Valongo," https://www.dgterritorio.gov.pt/dados-abertos, 2025, informação extraída da Planta de Ordenamento do PDM em vigor com aplicação da classificação e qualificação do solo estabelecida no Decreto Regulamentar n.º 15/2015 de 19 de agosto. [Cited on page 14.]

[38] ——, "SRUP – Rede Natura 2000 – Zonas de Proteção Especial," https://snig.dgterritorio.gov.pt/, 2021, servidão e Restrição de Utilidade Pública (SRUP) referente às Zonas de Proteção Especial (ZPE) em Portugal Continental, no âmbito da Rede Natura 2000. Define áreas prioritárias para conservação de habitats e espécies de aves selvagens, conforme a Diretiva Aves. [Cited on page 14.]

[39] ——, "Carta de Uso e Ocupação do Solo para 2018 (COS2018)," https://www.dgterritorio.gov.pt/Carta-de-Uso-e-Ocupacao-do-Solo-para-2018, 2020, mapa

temático da Direção-Geral do Território, concluído no final de 2019 e disponibilizado em 2020, referente à ocupação e uso do solo em Portugal Continental. [Cited on pages 14, 16, 21, and 28.]

[40] Direção-Geral do Património Cultural, “Património cultural arqueológico - sistema endovélico,” https://snig.dgterritorio.gov.pt/, 2025, conjunto de dados geográficos relativos a elementos patrimoniais de natureza arqueológica inventariados no sistema de informação Endovélico. [Cited on pages vi, 14, 19, and 26.]

[41] Instituto Nacional de Estatística, “Lugares 2001,” https://dados.gov.pt/es/datasets/lugares-2001/, 2025, dataset sobre aglomerados populacionais com dez ou mais alojamentos destinados à habitação de pessoas com designação própria, em Portugal Continental. [Cited on pages 14 and 20.]

[42] REN - Redes Energéticas Nacionais, “Mapa e caracterização da rede nacional de transporte de eletricidade (rnt),” https://datahub.ren.pt/pt/redes/rede-eletrica/, 2024, dados de 2024 sobre extensão das linhas, potência de transformação e infraestrutura da RNT. [Cited on pages 14 and 25.]

[43] OpenStreetMap contributors, “Openstreetmap changeset: 167746640 — modified highways near oe6d,” https://www.openstreetmap.org/changeset/167746640, 2025, edits by user KimberleyPlateau using JOSM/1.5, 9 days before access. [Cited on pages 14 and 19.]

[44] Direção-Geral de Energia e Geologia (DGEG), “Centrais solares de portugal continental,” https://snig.dgterritorio.gov.pt/ndg/srv/por/catalog.search#/metadata/d9fe8d62-416e-4c16-b760-c3a48a3b0388, 2016, dados abertos publicados no SNIG, com acesso via WMS e WFS. [Cited on page 14.]

[45] European Commission, “Regulamento (ue) n.º 493/2012 da comissão, de 11 de junho de 2012,” EUR-Lex, 2012, estabelece regras de execução para o cálculo dos rendimentos de reciclagem dos resíduos de pilhas e acumuladores, em conformidade com a Diretiva 2006/66/CE. [Online]. Available: https://eur-lex.europa.eu/legal-content/PT/TXT/?uri=CELEX:32012R0493 [Cited on page 16.]

[46] Junta de Andalucía, “Ley 2/1989, de 18 de julio, por la que se aprueba el inventario de espacios naturales protegidos de andalucía,” Boletín Oficial del Estado (BOE),

1989, y se establecen medidas adicionales para su protección. [Online]. Available: https://www.boe.es/buscar/act.php?id=BOE-A-1989-20636 [Cited on page 16.]

[47] J. M. Sánchez-Lozano, J. Teruel-Solano, P. L. Soto-Elvira, and M. Socorro García-Cascales, "Geographical Information Systems (GIS) and Multi-Criteria Decision Making (MCDM) methods for the evaluation of solar farms locations: Case study in south-eastern Spain," *Renewable and Sustainable Energy Reviews*, vol. 24, pp. 544–556, Aug. 2013. [Online]. Available: https://linkinghub.elsevier.com/retrieve/pii/S1364032113001780 [Cited on page 17.]

[48] M. Uyan, "GIS-based solar farms site selection using analytic hierarchy process (AHP) in Karapinar region, Konya/Turkey," *Renewable and Sustainable Energy Reviews*, vol. 28, pp. 11–17, Dec. 2013. [Online]. Available: https://linkinghub.elsevier.com/retrieve/pii/S1364032113004875 [Cited on page 17.]

[49] A. Alami Merrouni, F. Elwali Elalaoui, A. Mezrhab, A. Mezrhab, and A. Ghennioui, "Large scale PV sites selection by combining GIS and Analytical Hierarchy Process. Case study: Eastern Morocco," *Renewable Energy*, vol. 119, pp. 863–873, Apr. 2018. [Online]. Available: https://linkinghub.elsevier.com/retrieve/pii/S0960148117310078 [Cited on page 19.]

[50] República Portuguesa, "Lei n.º 107/2001, de 8 de setembro — lei de bases do património cultural," Procuradoria-Geral Distrital de Lisboa (PGDL), 2001, estabelece as bases da política e do regime de proteção e valorização do património cultural. [Online]. Available: https://www.pgdlisboa.pt/leis/lei_mostra_articulado.php?nid=844&tabela=leis [Cited on page 19.]

[51] Y. Noorollahi, H. Yousefi, and M. Mohammadi, "Multi-criteria decision support system for wind farm site selection using GIS," *Sustainable Energy Technologies and Assessments*, vol. 13, pp. 38–50, Feb. 2016. [Online]. Available: https://linkinghub.elsevier.com/retrieve/pii/S2213138815000788 [Cited on page 20.]

[52] A. Sohani, M. H. Shahverdian, H. Sayyaadi, and D. A. Garcia, "Impact of absolute and relative humidity on the performance of mono and poly crystalline silicon photovoltaics; applying artificial neural network," *Journal of Cleaner Production*, vol. 276, p. 123016, Dec. 2020. [Online]. Available: https://linkinghub.elsevier.com/retrieve/pii/S0959652620330614 [Cited on page 24.]

[53] Solar Energy Industries Association, “Solar energy,” https://www.seia.org/initiatives/about-solar-energy/, 2024, accessed: 2024-06-27. [Online]. Available: https://www.seia.org/initiatives/about-solar-energy/ [Cited on page 25.]

[54] Lumify Energy, “Making renewable energy simple,” https://lumifyenergy.com/, 2024, accessed: 2024-06-27. [Online]. Available: https://lumifyenergy.com/ [Cited on page 26.]

[55] L. Fouché. (2024) Le guide complet des fermes solaires. https://www.choisir.com/energie/articles/168782/le-guide-complet-des-fermes-solaires. Mis à jour le 17 janvier 2024. Consulté le 27 juin 2024. [Online]. Available: https://www.choisir.com/energie/articles/168782/le-guide-complet-des-fermes-solaires [Cited on page 26.]

[56] Corticeira Amorim, “The cork oak and natural cork play an instrumental role in the fight against climate changes,” 2014, accessed: 2025-06-30. [Online]. Available: https://www.amorim.com/en/media/news/the-cork-oak-and-natural-cork-play-an-instrumental-role-in-the-fight-against-climate-changes/1371/ [Cited on page 28.]

[57] Amorim Cork Solutions, “Cork oak forest,” 2024, accessed: 2025-06-30. [Online]. Available: https://www.amorimcorkflooring.us/cork-oak-forest [Cited on page 28.]

[58] S. Ribeiro, A. Cerveira, P. Soares *et al.*, “Natural regeneration of cork oak forests under climate change: a case study in portugal,” *Frontiers in Forests and Global Change*, vol. 7, p. 1332708, 2024. [Online]. Available: https://www.frontiersin.org/articles/10.3389/ffgc.2024.1332708/full [Cited on page 28.]

[59] R. M. Navarro-Cerrillo, F. J. Ruiz-Gómez, J. J. Camarero *et al.*, “Long-term carbon sequestration in pine forests under different silvicultural and climatic regimes in spain,” *Forests*, vol. 13, no. 3, p. 450, 2022. [Online]. Available: https://www.mdpi.com/1999-4907/13/3/450 [Cited on page 29.]

[60] P. J. López-Bellido *et al.*, “Assessment of carbon sequestration and the carbon footprint in olive groves in southern spain,” *Carbon Management*, 2016. [Cited on page 29.]

[61] I. Vourdoubas, “Estimation of carbon sequestration from olive tree groves in the island of crete, greece,” *International Journal of Agriculture and Environmental Research*, vol. 6, no. 4, pp. 553–560, 2020. [Cited on page 29.]

[62] A. Sofo *et al.*, “Potential for carbon sequestration in olive trees,” *Soil and Plant Research Reports*, 2005. [Cited on page 29.]

[63] M. Torrús-Castillo, J. Calero, and R. García-Ruiz, “Does olive cultivation sequester carbon?: Carbon balance along a c input gradient,” *Agriculture, Ecosystems Environment*, vol. 358, p. 108707, 2023. [Cited on page 29.]

[64] A. Brunori *et al.*, “Ecosystem services in vineyard landscapes,” *Carbon Balance and Management*, 2020. [Cited on page 29.]

[65] J. Villat and K. A. Nicholas, “Quantifying soil carbon sequestration from regenerative agricultural practices in crops and vineyards,” *Frontiers in Sustainable Food Systems*, 2023. [Cited on page 29.]

[66] M. D. Petrie *et al.*, “Grassland to shrubland state transitions enhance carbon sequestration in the northern chihuahuan desert,” *Global Change Biology*, 2015, fig. □based carbon exchange comparison, aumento de C em arbustos. [Cited on page 29.]

[67] S. Sow, S. Ranjan *et al.*, “Agroforestry and soil carbon sequestration: A nexus for system sustainability,” in *Agroforestry Solutions for Climate Change and Environmental Restoration*. Springer, 2024. [Cited on page 29.]

[68] T. J. Brandão *et al.*, “Maximizing tree carbon in croplands and grazing lands while improving ecosystem services,” *Carbon Balance and Management*, 2024. [Cited on page 29.]

[69] MDPI, “Solar panels and wildlife - lessening environmental impacts,” 2025, instalações em terras degradadas acarretam menor impacto em fauna. [Online]. Available: https://8msolar.com/... [Cited on page 29.]

[70] USDA Natural Resources Conservation Service, “Conservation considerations for solar farms,” Tech. Rep., 2024, diretrizes para vegetação sob painéis, conservação do solo e biodiversidade. [Online]. Available: https://www.nrcs.usda.gov/... [Cited on page 29.]

[71] G. A. Miller, “The magical number seven, plus or minus two: Some limits on our capacity for processing information,” *Psychological Review*, vol. 63, no. 2, pp. 81–97, 1956, originally presented at the Eastern Psychological Association, April 15, 1955. [Cited on page 33.]

[72] A. Emrouznejad and W. Ho, *Fuzzy Analytic Hierarchy Process*. Boca Raton: CRC Press, Taylor & Francis Group, 2017. [Cited on page 58.]

[73] Agência Portuguesa do Ambiente, "Parecer da Comissão de Avaliação – Nova Instalação Fotovoltaica para Autoconsumo (UPAC2) da Acuinova," https://sniaia.apambiente.pt/AIADOC/AIA3576/ptf_comissao_de_avaliacao_out_2021202210112717.pdf, October 2021, estudo de Impacte Ambiental (EIA). [Cited on pages 59 and 64.]

[74] Direção-Geral do Território, "Ortofotografias – Cartografia Topográfica," https://www.dgterritorio.gov.pt/cartografia/cartografia-topografica/ortofotos, 2025, accessed: 2025-07-01. [Cited on page 60.]

Appendix A — Full Set of Pairwise Comparison Matrices

This appendix contains the full set of pairwise comparison matrices developed for the Analytic Hierarchy Process (AHP) model, including:

- Criteria-level comparisons within each factor.
- Subcriteria comparisons for each classification criterion (CC1–CC9).

Table 1: Pairwise comparison matrix of the criteria within Factor F2 (Climatic).

	CC3 (Relative Humidity)
CC3	1

Table 2: Pairwise comparison matrix of the criteria within Factor F3 (Location).

	CC4 (Roads)	CC5 (Power Grid)	CC6 (Parcel Size)
CC4	1	2	3
CC5	1/2	1	2
CC6	1/3	1/2	1

Table 3: Pairwise comparison matrix of the criteria within Factor F4 (Orography).

	CC7 (Slope)	CC8 (Orientation)
CC7	1	1.5
CC8	1/1.5	1

Table 4: Pairwise comparison matrix of the criteria within Factor F5 (Environmental).

	CC9 (Land Use)
CC9	1

Table 5: Pairwise comparison matrix of subcriteria for CC2 (PVOUT).

	≤900	900–1100	1100–1200	1200–1300	1300–1400	1400–1500	1500–1600	1600–1700	>1700
≤900	1	1/2	1/3	1/4	1/5	1/6	1/7	1/8	1/9
900–1100	2	1	1/2	1/3	1/4	1/5	1/6	1/7	1/8
1100–1200	3	2	1	1/2	1/3	1/4	1/5	1/6	1/7
1200–1300	4	3	2	1	1/2	1/3	1/4	1/5	1/6
1300–1400	5	4	3	2	1	1/2	1/3	1/4	1/5
1400–1500	6	5	4	3	2	1	1/2	1/3	1/4
1500–1600	7	6	5	4	3	2	1	1/2	1/3
1600–1700	8	7	6	5	4	3	2	1	1/2
>1700	9	8	7	6	5	4	3	2	1

Table 6: Pairwise comparison matrix for subcriteria of CC3 (Relative Humidity %).

	≤65	65–70	70–75	75–79	>79
≤65	1	2	3	4	5
65–70	1/2	1	1.5	2	2.5
70–75	1/3	2/3	1	1.5	2
75–79	1/4	1/2	2/3	1	1.5
>79	1/5	2/5	1/2	2/3	1

Table 7: Pairwise comparison matrix for subcriteria of CC4 (Proximity to roads in meters).

	≤100	100–1000	1000–3000	3000–5000	>5000
≤100	1	1/7	1/5	1/3	1
100–1000	7	1	3	5	7
1000–3000	5	1/3	1	2	5
3000–5000	3	1/5	1/2	1	3
>5000	1	1/7	1/5	1/3	1

Table 8: Pairwise comparison matrix for subcriteria of CC5 (Proximity to electric grid in meters).

	$\leq$1000	1000–3000	3000–6000	6000–10000	$>$10000
$\leq$1000	1	3	5	7	9
1000–3000	1/3	1	3	5	7
3000–6000	1/5	1/3	1	3	5
6000–10000	1/7	1/5	1/3	1	3
$>$10000	1/9	1/7	1/5	1/3	1

Table 9: Pairwise comparison matrix for subcriteria of CC6 (Required Area in hectares).

	$<$6	$\geq$6
$<$6	1	1/9
$\geq$6	9	1

Table 10: Pairwise comparison matrix for subcriteria of CC7 (Slope %).

	$\leq$3	3–5	5–7	7–9	9–11	11–13	13–14	$>$14
$\leq$3	1	3	4	5	6	7	8	9
3–5	1/3	1	3	4	5	6	7	8
5–7	1/4	1/3	1	3	4	5	6	7
7–9	1/5	1/4	1/3	1	3	4	5	6
9–11	1/6	1/5	1/4	1/3	1	3	4	5
11–13	1/7	1/6	1/5	1/4	1/3	1	3	4
13–14	1/8	1/7	1/6	1/5	1/4	1/3	1	3
$>$14	1/9	1/8	1/7	1/6	1/5	1/4	1/3	1

Table 11: Pairwise comparison matrix of subcriteria for CC8 (Orientation, °)

	158–202	112–158	202–248	248–292	292–315	45–112	>315	<45
158–202	1	3	3	5	5	5	9	9
112–158	1/3	1	1	3	3	3	7	7
202–248	1/3	1	1	3	3	3	7	7
248–292	1/5	1/3	1/3	1	1	1	5	5
292–315	1/5	1/3	1/3	1	1	1	5	5
45–112	1/5	1/3	1/3	1	1	1	5	5
>315	1/9	1/7	1/7	1/5	1/5	1/5	1	1
<45	1/9	1/7	1/7	1/5	1/5	1/5	1	1

Table 12: Pairwise comparison matrix of subcriteria for CC9 (Land Use Impact Level)

	Minimum	Low	Medium-Low	Medium	Medium-High	High
Minimum	1	2	6	7	8	9
Low	1/2	1	2	6	7	8
Medium-Low	1/6	1/2	1	2	6	7
Medium	1/7	1/6	1/2	1	2	6
Medium-High	1/8	1/7	1/6	1/2	1	2
High	1/9	1/8	1/7	1/6	1/2	1